Synthesis and Evaluation of Technetium-99m- and Rhenium-Labeled Inhibitors of the Prostate-Specific Membrane Antigen (PSMA)

Sangeeta R. Banerjee,[†] Catherine A. Foss,[†] Mark Castanares,[‡] Ronnie C. Mease,[†] Youngjoo Byun,[†] James J. Fox,[†] John Hilton,[†] Shawn E. Lupold,[§] Alan P. Kozikowski,[||] and Martin G. Pomper*[,†,‡]

Russell H. Morgan Department of Radiology and Radiological Sciences, Department of Pharmacology & Molecular Sciences, Department of Urology, Johns Hopkins Medical Institutions, Baltimore, Maryland 21231, and Department of Medicinal Chemistry and Pharmacognosy, University of Illinois at Chicago, Illinois 60612

Received February 2, 2008

The prostate-specific membrane antigen (PSMA) is increasingly recognized as a viable target for imaging and therapy of cancer. We prepared seven ^{99m}Tc/Re-labeled compounds by attaching known Tc/Re chelating agents to an amino-functionalized PSMA inhibitor (lys-NHCONH-glu) with or without a variable length linker moiety. K_i values ranged from 0.17 to 199 nM. Ex vivo biodistribution and in vivo imaging demonstrated the degree of specific binding to engineered PSMA+ PC3 PIP tumors. PC3-PIP cells are derived from PC3 that have been transduced with the gene for PSMA. Despite demonstrating nearly the lowest PSMA inhibitory potency of this series, $[^{99m}Tc(CO)_3(\mathbf{L1})]^+$ ($\mathbf{L1}$ = (2-pyridylmethyl)$_2$N(CH$_2$)$_4$CH(CO$_2$H)-NHCO-(CH$_2$)$_6$CO-NH-lys-NHCONH-glu) showed the highest, most selective PIP tumor uptake, at 7.9 ± 4.0% injected dose per gram of tissue at 30 min postinjection. Radioactivity cleared from nontarget tissues to produce a PIP to flu (PSMA-PC3) ratio of 44:1 at 120 min postinjection. PSMA can accommodate the steric requirements of ^{99m}Tc/Re complexes within PSMA inhibitors, the best results achieved with a linker moiety between the ε amine of the urea lysine and the chelator.

Introduction

Prostate cancer (PCa) is the leading cancer in the U.S. population and the second leading cause of cancer-related death in men.[1] By the time of diagnosis, only one-half of PCa tumors are clinically localized and one-half of those represent extracapsular spread. Currently anatomic methods, such as computed tomography (CT), magnetic resonance (MR) imaging, and ultrasound, predominate for clinical imaging of prostate cancer. The radiolabeled monoclonal antibody [^{111}In]ProstaScint has also been used, however, this agent tends to produce images that are challenging to interpret.[2–4] Low-molecular-weight, radiopharmaceutical-based imaging agents may provide superior pharmacokinetics for imaging than radiolabeled antibodies, which tend to have long circulation times and delayed clearance from nontarget tissues. A variety of experimental low-molecular-weight PCa imaging agents are currently being pursued clinically, including radiolabeled choline analogues,[5–9] [^{18}F]fluorodihydrotestosterone ([^{18}F]FDHT),[10] anti-1-amino-3-[^{18}F]-fluorocyclobutyl-1-carboxylic acid (anti[^{18}F]F-FACBC),[11] [^{11}C]acetate, and 1-(2-deoxy-2-[^{18}F]fluoro-L-arabinofuranosyl)-5-methyluracil ([^{18}F]FMAU).[12] Each operates by a different mechanism and has certain advantages, e.g., low urinary excretion for [^{11}C]choline, and disadvantages, such as the short physical half-life of positron-emitting radionuclides. A promising new series of low-molecular-weight imaging agents targets the prostate-specific membrane antigen (PSMA).[13–16]

PSMA is a type II integral membrane protein that has abundant and restricted expression on the surface of PCa, particularly in androgen-independent, advanced, and metastatic disease.[17] The latter is important because almost all PCa becomes androgen independent. It is also expressed within the endothelium of most solid tumors other than prostate.[18] PSMA possesses the criteria of a promising target for therapy, i.e., abundant and restricted (to prostate) expression at all stages of the disease, presentation at the cell surface but not shed into the circulation, and association with enzymatic or signaling activity.[17] The PSMA gene is located on the short arm of chromosome 11 and functions both as a folate hydrolase and neuropeptidase. It is the neuropeptidase function that is equivalent to glutamate carboxypeptidase II (GCPII), which is referred to as the "brain PSMA",[17] and may modulate glutamatergic transmission by cleaving *N*-acetylaspartylglutamate (NAAG) to *N*-acetylaspartate (NAA) and glutamate.[19] There are up to 10^6 PSMA molecules per cancer cell, further suggesting it as an ideal target for imaging and therapy with radionuclide-based techniques.[20]

Recently, we have demonstrated selective imaging of xenografts that express PSMA using small animal positron emission tomography (PET) and single photon emission computed tomography (SPECT) and the urea-based PSMA inhibitors *N*-[*N*-[(*S*)-1,3-dicarboxypropyl]carbamoyl]-(*S*)-[^{11}C]methyl-L-cysteine, [^{11}C]DCMC, *N*-[*N*-[(*S*)-1,3-dicarboxypropyl]carbam-

* To whom correspondence should be addressed. Phone: 410-955-2789. Fax: 443-817-0990. E-mail: mpomper@jhmi.edu. Address: Martin G. Pomper, M.D., Ph.D., Johns Hopkins Medical Institutions, 1550 Orleans Street, 492 CRB II, Baltimore, MD 21231.

[†] Russell H. Morgan Department of Radiology and Radiological Sciences, Johns Hopkins Medical Institutions.

[‡] Department of Pharmacology & Molecular Sciences, Johns Hopkins Medical Institutions.

[§] Department of Urology, Johns Hopkins Medical Institutions.

[||] Department of Medicinal Chemistry and Pharmacognosy, University of Illinois at Chicago.

[a] Abbreviations: PSMA, prostate-specific membrane antigen; GCPII, glutamate carboxypeptidase II; NAALADase, *N*-acetylated-α-linked acidic dipeptidase; DCMC, *N*-[*N*-[(*S*)-1,3-dicarboxypropyl]carbamoyl]-(*S*)-methyl-L-cysteine; DCIT, *N*-[*N*-[(*S*)-1,3-dicarboxypropyl]carbamoyl]-(*S*)-3-iodo-L-tyrosine; DCFBC, and *N*-[*N*-[(*S*)-1,3-dicarboxypropyl]carbamoyl]-(*S*)-4-fluorobenzyl-L-cysteine; SAAC, single amino acid chelate; DCL, *N*-[*N*-[(*S*)-1,3-dicarboxypropyl]carbamoyl]-(*S*)-L-lysine; PMPA, 2-(phosphonomethyl)pentanedioic acid.

10.1021/jm800111u CCC: $40.75
Published on Web 07/19/2008

Chart 1. Urea-Based PSMA Inhibitors[a]

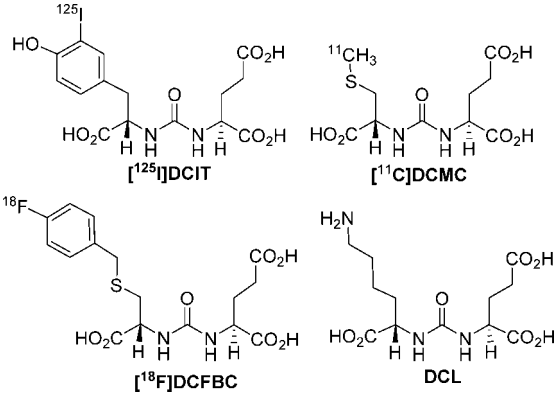

[a] [^{125}I]DCIT = *N*-[*N*-[(*S*)-1,3-dicarboxypropyl]carbamoyl]-(*S*)-3-[^{125}I]iodo-L-tyrosine, [^{11}C]DCMC = *N*-[*N*-[(*S*)-1,3-dicarboxypropyl]carbamoyl]-(*S*)-[^{11}C]methyl-L-cysteine, [^{18}F]DCFBC = *N*-[*N*-[(*S*)-1,3-cicarboxypropyl]carbamoyl]-(*S*)-4-[^{18}F]fluorobenzyl-L-cysteine, DCL = *N*-[*N*-[(*S*)-1,3-dicarboxypropyl]carbamoyl]-(*S*)-lysine.

oyl]-*(S)*-3-[^{125}I]iodo-L-tyrosine, [^{125}I]DCIT, and *N*-[*N*-[(*S*)-1,3-dicarboxypropyl]carbamoyl]-(*S*)-4-[^{18}F]fluorobenzyl-L-cysteine, [^{18}F]DCFBC (Chart 1).[13–15] These results encouraged us to investigate the possibility of developing ^{99m}Tc-labeled, urea-based inhibitors as PCa imaging agents. Although positron-emitting radionuclides are increasingly used in clinical medicine, ^{99m}Tc remains the radionuclide of choice for clinical scintigraphic imaging because of its favorable physical properties ($t_{1/2}$ = 6 h, E_γ = 140 keV), low cost, and widespread availability. The development of technetium complexes as radiopharmaceuticals is facilitated by the use of rhenium, the group VIIB congener of technetium. Rhenium generally produces complexes with similar physical properties to those of technetium and is often used as a nonradioactive alternative to technetium for large-scale synthesis and structural characterization.

Here we describe the development of low-molecular-weight, urea-based inhibitors incorporating tridentate chelators for binding of the $\{M(CO)_3\}^+$ core, (M = ^{99m}Tc, ^{186,188}Re), while retaining high affinity to PSMA. Because of high stability and favorable labeling characteristics, the organometallic Re(I)$(CO)_3$/^{99m}Tc(I)$(CO)_3$ approach represents an attractive radiolabeling strategy. A number of tridentate chelates with different sets of nitrogen, sulfur, oxygen donor atoms are known to form highly stable complexes with the $\{M(CO)_3\}^+$ cores.[21,22] Among them, the single amino acid chelate concept,[23,24] (SAAC), has proved useful for designing our new urea-based inhibitors. We describe the synthesis and in vitro binding of seven ^{99m}Tc/Re-based radiopharmaceuticals formed from ligands **L1**−**L7** (Chart 2) as well as ex vivo biodistribution and in vivo imaging studies of selected agents.

Chemistry

Structure-Based Design of PSMA Binding Inhibitors. Recently, several high-resolution X-ray crystal structures of GCPII (PSMA) with known, low-molecular-weight, glutamate-containing inhibitors of PSMA have been reported.[25–28] Those structural studies established that the binding site of PSMA contains a binuclear zinc ion and two substrate binding pockets, i.e., an S1 (nonpharmacophore) pocket and an S1′ (pharmacophore) pocket. The active site also contains a chloride ion in the S1 pocket. In the vicinity of the S1 pocket resides a funnel-shaped tunnel with a depth of approximately 20 Å and a width of 8−9 Å.[25] Similarly, a narrow cavity is present near the S1′ pocket.[27] Moreover, it has been determined that the glutamate

Chart 2. Urea-Based PSMA Ligands **L1**−**L7**

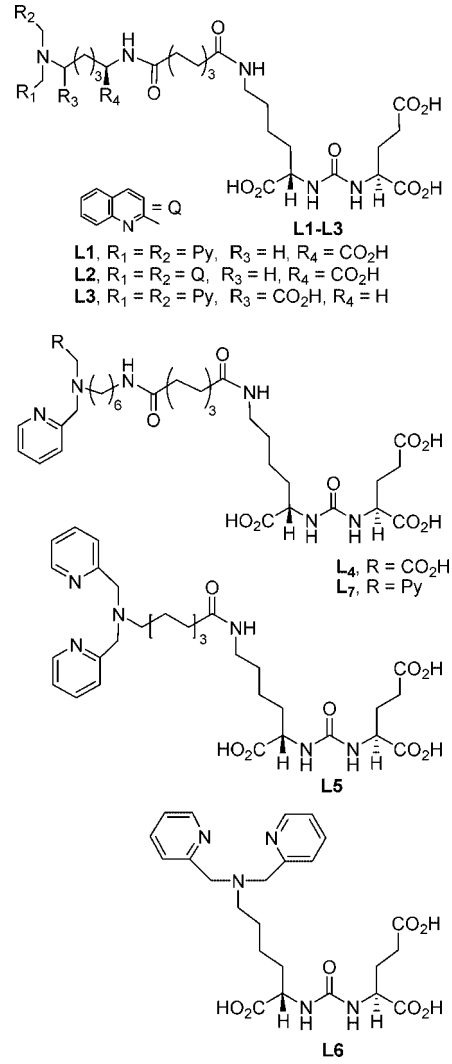

moiety of the inhibitors has a predisposition to orient within the narrow S1′ pocket, whereas the remainder of the molecule resides within the large S1 pocket. These observations are similar for PSMA X-ray crystal structures upon cocrystallization with compounds in the urea series, namely, DCMC, DCIT, and DCFBC (Chart 1) (data not shown). In the current study, we sought to synthesize a conjugate between a glutamate-containing, urea-based inhibitor and known chelators of $[Re(I)(CO)_3]^+$/$[^{99m}Tc(I)(CO)_3]^+$. In the design of these new conjugates, it was important to optimize the interaction between PSMA and the bulky chelator. Considering the ∼9 Å diameter of the rhenium tricarbonyl and technetium tricarbonyl coordination spheres with pyridyl-based chelates, determined from reported X-ray crystal structures,[29,30] the calculated average volume of the metal tricarbonyl core with the bispyridyl chelate was found to be ∼378 Å^3. To enable high-affinity binding of our putative imaging agents to PSMA, we envisioned the need to attach a functionalized methylene linker (>20 Å) to the remainder of the molecule from the α-carbon of the urea function. Accordingly, we have designed three sets of compounds, each with a different linker length: **L1**−**L3**, with a linker of ∼31.5 Å, **L4** and **L7**, with linker length of ∼33 Å, and **L5** and **L6**, with linker lengths of ∼22 Å and 7.7 Å, respectively (Chart 2). We hypothesized that the metal chelate portion of the compound should remain outside of the 20 Å tunnel as long as the

Scheme 1

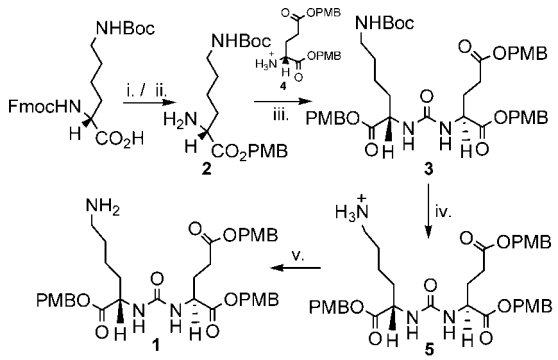

PMB = *p*-methoxy benzyl group; i. 4-methoxybenzyl chloride, Cs_2CO_3, DMF, rt, 4h; ii. 20% piperidine, DMF, rt, 20 min; iii.Triphosgene, NEt_3, CH_2Cl_2, -80°C to rt; iv. TsOH, Ethanol, ethyl acetate, rt, 2h; v. 0.5 (N) $NaHCO_3$.

glutamate moiety is maintained within the S1′ pocket, permitting interaction between the inhibitor and PSMA.

Synthesis of Urea-linked Chelators. We elected to develop a new series of PSMA inhibitors containing lysine (Chart 1, DCL) in order to utilize the free ε amine of lysine for conjugation or derivatization with a suitable metal chelating group. Compound **1** (Scheme 1) is a key intermediate, integral to synthesis of all of the putative imaging agents described. The protected lysine analogue **2** was prepared in two steps. Commercially available N_ε-Boc-N_α-Fmoc-L-lysine was reacted with 4-methoxybenzyl chloride and cesium carbonate in *N*, *N*-dimethylformamide (DMF), followed by removal of the Fmoc group using 20% piperidine in DMF. Flash chromatography provided the desired compound **2** in 80% yield. Urea **3** was obtained by treating bis-4-methoxybenzyl-L-glutamate·HCl, **4** [31,32] with triphosgene and triethylamine at −78 °C followed by in situ trapping of the isocyanate intermediate by addition of **2**. Selective cleavage of the *N*-Boc group of **3** with *p*-toluenesulfonic acid in ethanol/ethyl acetate[33,34] produced **5**. Basic extraction of a solution of **5** in CH_2Cl_2 gave the free base **1**. The *p*-methoxybenzyl (PMB) group was conveniently removed at room temperature by using trifluoroacetic acid (TFA)/anisole or TFA/CH_2Cl_2 solution in the final step after performing the required conjugation.

The synthesis of the chelators and their conjugation with intermediate **1** are presented in Schemes 2–6. Compound **1** was used to attach different linkers as well as metal chelators to generate a new series of PSMA inhibitors, **L1**−**L7**, for coordination of $\{^{99m}Tc(CO)_3\}^+/\{Re(CO)_3\}^+$. Key *N*-hydroxysuccinimide (NHS) ester intermediate **6**, shown in Scheme 2, was prepared by conjugation of **1** with excess disuccinimidyl suberate (DSS) in DMF. Compound **6** was then reacted with three different bispyridyl chelators, **7**, **9**, and **13**, a bisquinoline chelator, **8**, and a monopyridyl monoacid chelator, **11**, to prepare **L1**−**L4,** and **L7**. Chelators **7**, **8**, **9**, and **13** were prepared according to published procedures.[35]

Synthesis of the monopyridyl monoacid chelator was performed by modification of a previously described procedure (Scheme 3). Compound **10** was prepared according to a previously reported method.[36] Reductive amination of **10**, using glyoxylic acid in presence of sodium triacetoxyborohydride in dichloroethane, followed by removal of the protecting group using a solution of TFA/CH_2Cl_2 at ambient temperature, produced **11**. The synthesis of **L5** is outlined in Scheme 4. Compound **12** was prepared by reductive amination of commercially available 8-aminocaproic acid with pyridine-2-carboxaldehyde and sodium triacetoxyborohydride followed by NHS ester formation with *N*-hydroxysuccinimide in the presence of *O*-benzotriazole-*N*,*N*,*N*′,*N*′-tetramethyl-uronium-hexafluorophosphate (HBTU). Compound **L5** was obtained by reacting **12** with **5** in CH_2Cl_2 and triethylamine, followed by deprotection of the PMB groups using TFA/CH_2Cl_2. Compound **L6** was prepared by reductive amination of **1** using pyridine-2-carboxaldehyde and sodium triacetoxyborohydride followed by deprotection of the PMB groups using TFA/CH_2Cl_2 (Scheme 5).

Synthesis of Rhenium Analogs (ReL1−ReL7). Synthesis of compounds $[Re(CO)_3L]^{+/0}$ (L = **L1**−**L7**) was performed by ligand exchange reaction using the rhenium tricarbonyl precursor $[Re(CO)_3(H_2O)_3]Br$[37] as shown in Scheme 6 for **L1**. Equimolar quantities of the ligand (**L1**−**L7**) and the precursor were refluxed under argon for 3 h to afford the corresponding rhenium complex in quantitative yield in each case. The complexation was monitored by high-performance liquid chromatography (HPLC). All complexes were purified via HPLC and characterized by standard spectroscopic methods.

Modeling of L1 in the Active Site of PSMA. For molecular modeling studies of **L1** with PSMA, a recently published crystal structure of PSMA in complex with (*S*)-2-(4-iodobenzylphosphonomethyl)-pentanedioic acid (GPI-18431) (PDB ID: 2C6C) was used.[25] Initially, we carried out docking studies of **L1** with the active site of 2C6C using LigandFit and CHARMm-based CDOCKER protocols implemented in Discovery Studio 1.7 (DS 1.7, Accelrys Inc.). However, none of them produced docked poses in the active site because of the bulkiness of **L1**. Therefore, we employed an alternative way to elucidate a potential binding mode of **L1**. PSMA crystal structures with several ligands including GPI-18431, 2-(phosphonomethyl)pentanedioic acid (2-PMPA) and glutamate showed that the glutamate portion of these compounds within the S1′-pocket virtually overlap, suggesting that the orientation of the glutamate moiety is unchanged despite a variety of structural motifs concurrently within the S1-pocket. That was no surprise, as we expected the glutamate portion of **L1** to orient in the S1′-pocket in a fashion similar to that of the known PSMA inhibitors (e.g., GPI-18431 and 2-PMPA). In particular, the α-carboxylate of glutamate, which interacts with Arg 210, is known to be essential for PSMA binding.[38] We superimposed **L1** with GPI-18431 using four tether attachment points in glutamate (*N*-*C*H(*C*OO$^-$)-*C*H$_2$, see Supporting Information, Figure 1). Coordinates of the superimposed **L1** were transferred and merged in the apo-form of 2C6C in which the ligand GPI-18431 was removed.

Molecular dynamics simulation of the merged PSMA/**L1** complex was performed with Generalized Born with a simple Switching (GBSW) as an implicit solvent model. Amino acid residues within 7 Å of **L1** remained flexible while all other amino acids were constrained. As shown in Supporting Information Figure 2 (see Supporting Information), the location of the carboxylic acid in the lysine portion of **L1** dramatically changed and strongly interacted with two arginines (Arg 534 and Arg 536, Figure 1A) after molecular dynamics simulation, while the two carboxylic acids of glutamate changed only slightly. The linear-type linker of initial **L1** was grooved for maximizing interaction with the tunnel region of PSMA, i.e., the flexible linear-type linker of initial **L1** adopted a compact conformation, thus enhancing the interaction of **L1** with the tunnel region of PSMA after molecular dynamics simulations (Figure 1B and Supporting Information Figure 2). From this PSMA/**L1** model, the α-carboxylate of glutamate demonstrated hydrogen bonding interactions with Arg 210, Tyr 552, and Tyr 700 and the γ-carboxylate did similarly with Asn 257 and Lys 699. In

Scheme 2

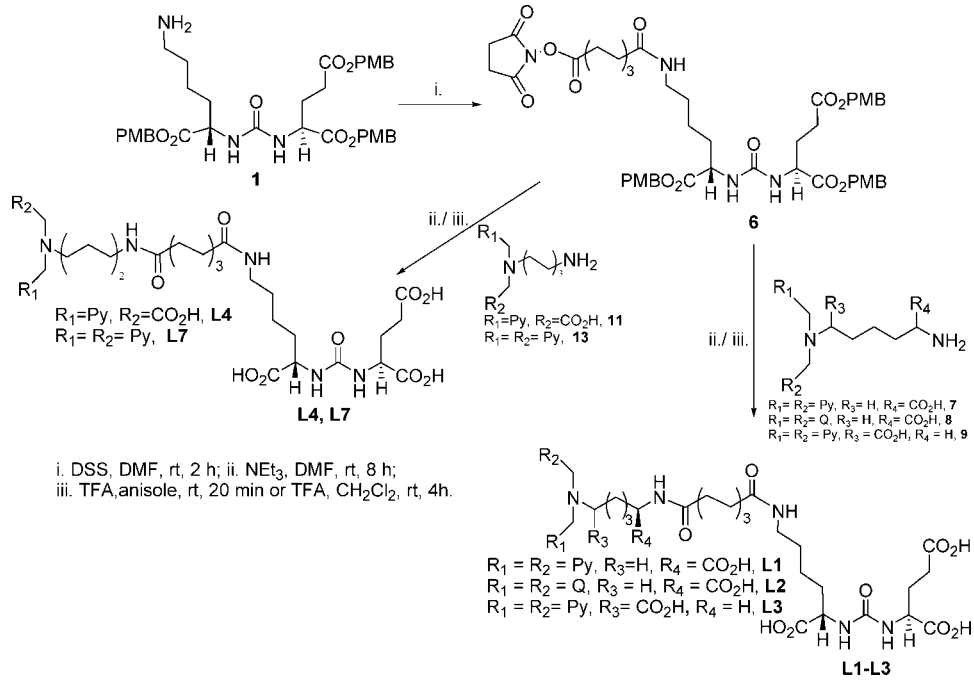

i. DSS, DMF, rt, 2 h; ii. NEt_3, DMF, rt, 8 h;
iii. TFA,anisole, rt, 20 min or TFA, CH_2Cl_2, rt, 4h.

Scheme 3

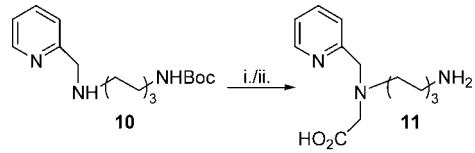

i. glyoxylic acid, $NaBH(OAc)_3$, CH_2Cl_2, rt, 16h;
ii. TFA, CH_2Cl_2, rt, 4h.

Scheme 4

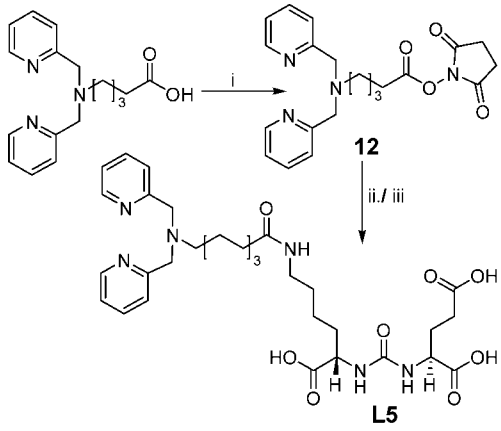

i. N-hydroxysuccinimide, HBTU, DMF, 16 h;
ii. **5**, NEt_3, CH_2Cl_2; iii. TFA, CH_2Cl_2, 4h, 73%.

addition, the two NH groups of the urea contribute to interaction with Gly 518.

Radiochemistry. Radiolabeling with $[^{99m}Tc(CO)_3(OH_2)_3]^+$ was performed using the commercially available Isolink kit at ligand concentrations of $10^{-5}-10^{-6}$ M with incubation times of 30 min at 95 °C. Adducts were produced in high radiochemical yield (>70%) and purity (>98%). Formation of the $[^{99m}Tc(CO)_3L]^{+/0}$ (Tc**L1**−Tc**L7**) complexes resulted in a significant shift in the HPLC retention times (to longer) compared

Scheme 5

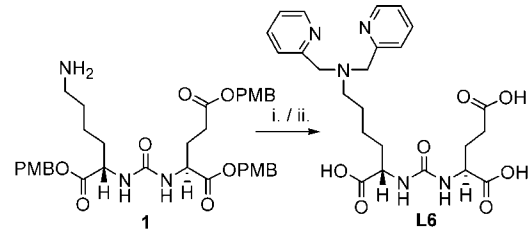

i. pyridine-2-carboxaldehyde, $NaBH(OAc)_3$, CH_2Cl_2, rt, 4h;
ii. TFA, CH_2Cl_2, rt, 2h.

Scheme 6

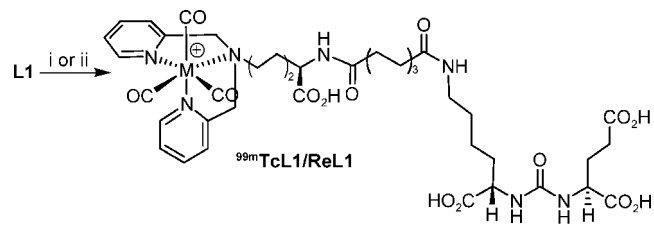

i. $[Tc(CO)_3(H_2O)_3]^+$, pH 7.2, 95°C, 30 min;
ii. $[NEt_4]_2[ReBr_3(CO)_3]$, 90°C, 4h.

to those of the free ligands and $[^{99m}Tc(CO)_3(OH_2)_3]^+$, enabling the clear separation of the radiotracers.

Electronic Properties of ReL2. Bisquinoline ligand **L2** allows for the preparation of isostructural fluorescent $\{Re(CO)_3\}^+$ core complexes and radioactive $\{^{99m}Tc(CO)_3\}^+$ core complexes. Consequently, the fluorescent properties of Re**L2** were investigated to determine whether the rhenium-based complexes possess suitable characteristics for use as biological probes.[39,40] The electronic spectrum of Re**L2** exhibited absorbance at 321 nm with an extinction coefficient of 17200 M^{-1}. Excitation of Re**L2** at 321 nm provides an intense fluorescence emission at 550 nm. The large Stokes shift is characteristic of this class of fluorophore.[41] The emission peak is assigned to a

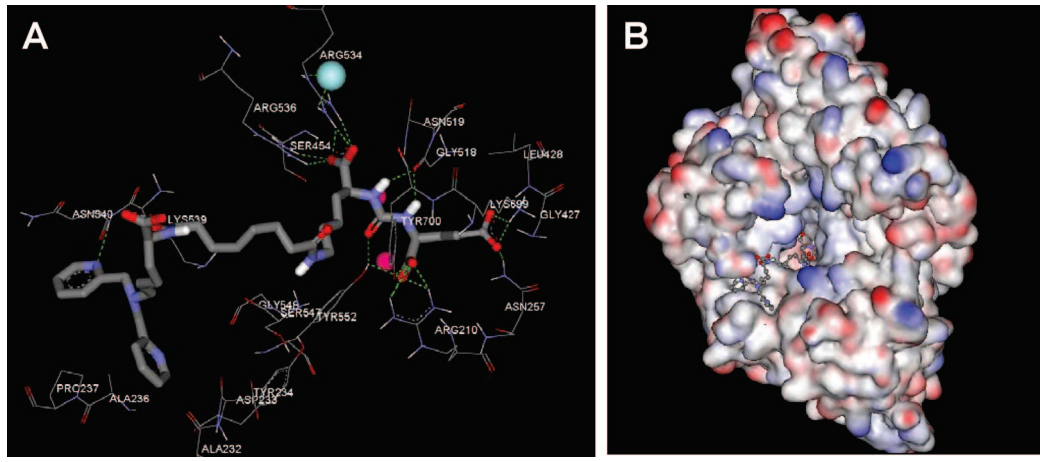

Figure 1. Binding mode of **L1** to the active site of PSMA (A). The corresponding contour map is shown in (B).

Table 1. PSMA Inhibitory Activity and Calculated ClogD

	K_i [nM]	95% CI[a]	ClogD
L1	15.25	7.93	−7.69
Re**L1**	10.75	3.81	
L2	0.17	0.05	−3.91
Re**L2**	0.50	0.07	
L3	1.08	0.14	−7.19
Re**L3**	10.34	3.76	
L4	2.54	0.60	−6.13
Re**L4**	0.17	0.08	
L5	1.86	0.21	−5.05
Re**L5**	0.91	0.44	
L6	7.53	5.65	−6.25
Re**L6**	199.56	135.26	
L7	0.45	0.25	−5.61
Re**L7**	2.06	0.25	
PMPA	0.20	0.06	−8.65

[a] Confidence interval.

^{3}MLCT [dπ(Re) → π*(ligand)] excited state on the basis of previous spectroscopic studies of Re(I) tricarbonyl complexes.[41–44] The fluorescence lifetime for Re**L2** is 11.8 μs (λ_{em} = 550 nm) in ethylene glycol under an argon atmosphere, which is sufficiently long to overcome the effects of endogenous fluorescence. Cellular autofluorescence can complicate in vitro imaging studies, however, because it occurs on the nanosecond time scale, it can be eliminated using time-gating techniques so long as the probe under investigation has a sufficiently long lifetime. The fluorescence quantum yield of Re**L2** of 0.018 in ethylene glycol under argon is low but comparable to those reported for other transition-metal band fluorescence probes.[44,45]

Biological Results

In Vitro Binding Studies. The relative binding affinities of **L1**−**L7** and Re**L1**−Re**L7** were determined using the *N*-acetylated-α-linked acidic dipeptidase (NAALADase) assay as previously described.[46,47] The data are presented in Table 1, with corresponding structures shown in Chart 2. As all compounds possess the lys-NHCONH-glu motif, structural variation derives from (a) the length of the linker between the chelator and the amide carbonyl carbon attached to the lysine moiety, (b) the chelator, which may be either the bispyridyl, bisquinoline, or mixed (monopyridyl monocarboxyl) functional groups, (c) the presence or absence of a second amide function between the chelator and the first amide—attached to the lysine moiety, and (d) the presence or absence of a carboxyl group either adjacent to the chelator or adjacent to the second (linker) amide group. Immediately evident is the need for a methylene chain length longer than that provided by lysine itself, as the Re-chelated version of **L6** displays the lowest PSMA inhibitory activity of all compounds measured and was not capable of imaging PMSA+ tumors (data not shown). Compound **L5** demonstrates that linkers containing seven methylene units between the chelator nitrogen and the amide carbonyl provide compounds of low nanomolar K_i. Longer linkers can also be accommodated easily (**L4** and **L7**). Introduction of rhenium does not cause a consistent change in inhibitory activity with Re-labeled versions only of **L1**, **L4**, and **L5**, demonstrating higher inhibitory activities than the corresponding unchelated compounds. Introduction of the $Re(CO)_3$ core/moiety to chelators of this class forces the chelator into a facial configuration, with unpredictable effects on binding to the active site. Placing the carboxylate adjacent to the chelator (**L3**), rather than adjacent to the amide nitrogen on the linker (**L1**) caused an increase in inhibitory activity of over an order of magnitude for the unchelated versions, although the Re-labeled versions were comparable. The bisquinoline chelator, which is much less polar than the bispyridyl, provides correspondingly stronger PSMA inhibitory activity. Replacing one of the pyridines with a carboxylic acid moiety (**L7** to **L4**) causes a 6-fold increase in inhibitory activity for the unchelated molecules but a 12-fold decrease in activity for the more biologically relevant Re-labeled compounds. Because of the many structural perturbations provided in this small structure−activity series, it is difficult to determine the effect of linker chain length other than to say that a linker beyond the lysine moiety itself is necessary for productive interaction with PSMA.

Ex Vivo Biodistribution. Compounds [^{99m}Tc]**L1**−**L3** were assessed for their pharmacokinetics ex vivo in severe-combined immunodeficient (SCID) mice bearing both PSMA+ PC3 PIP and PSMA−flu xenografts.[14,18] Tables 2–4 show the percent injected dose per gram (%ID/g) uptake values in selected organs for compounds [^{99m}Tc]**L1**−**L3**, respectively. Compound [^{99m}Tc]**L1** showed clear PSMA-dependent binding in PC3 PIP tumor xenografts, reaching a maximum uptake, among times investigated, of 7.87 ± 3.95%ID/g at 30 min postinjection (pi). PSMA+ tumor to PSMA− tumor (PIP:flu) uptake ratios ranged from 23 at 30 min pi to a high of 68 at 300 min pi. The distribution within normal organs and tissues was also favorable, with low nonspecific tissue uptake and rapid clearance. The highest nonspecific uptake observed was in the spleen at 30 min pi and was 10.59 ± 6.05%ID/g, which decreased to 1.81 ± 1.10 by 60 min pi. Kidney uptake, chiefly due to high expression of PSMA within proximal tubules,[48] was expectedly

Table 2. Biodistribution of [^{99m}Tc]**L1** in Tumor Bearing Mice[a]

	30 min	60 min	120 min	300 min
blood	0.54 ± 0.39	0.11 ± 0.04	0.02 ± 0.01	0.01 ± 0.00
heart	0.19 ± 0.13	0.04 ± 0.02	0.02 ± 0.01	0.01 ± 0.00
lung	0.64 ± 0.23	0.18 ± 0.06	0.05 ± 0.00	0.04 ± 0.06
liver	1.49 ± 1.12	0.25 ± 0.15	0.08 ± 0.04	0.04 ± 0.01
stomach	0.35 ± 0.15	0.17 ± 0.00	0.41 ± 0.61	0.03 ± 0.01
pancreas	0.18 ± 0.10	0.05 ± 0.02	0.01 ± 0.01	0.00 ± 0.00
spleen	10.59 ± 6.05	1.81 ± 1.10	0.59 ± 0.29	0.07 ± 0.04
fat	0.36 ± 0.14	0.11 ± 0.03	0.05 ± 0.07	0.01 ± 0.00
kidney	95.66 ± 22.06	68.54 ± 8.32	10.08 ± 5.71	1.26 ± 0.67
muscle	0.39 ± 0.12	0.25 ± 0.15	0.056 ± 0.04	0.04 ± 0.05
small intestine	5.87 ± 2.35	1.29 ± 0.76	0.38 ± 0.13	0.03 ± 0.01
large intestine	2.28 ± 2.03	16.02 ± 12.39	1.30 ± 2.00	0.10 ± 0.09
bladder	2.31 ± 0.88	2.19 ± 1.78	5.01 ± 8.18	0.80 ± 1.33
PC-3 PIP	7.87 ± 3.95	3.86 ± 0.57	2.31 ± 0.84	0.84 ± 0.51
PC-3 flu	0.34 ± 0.15	0.16 ± 0.08	0.05 ± 0.02	0.01 ± 0.01
PIP:muscle	20	15	41	23
flu:muscle	0.9	0.6	0.9	0.3
PIP:flu	23	25	44	68

[a] Values expressed are in % ID/g ± standard deviation. $N = 4$ for all tissues.

Table 3. Biodistribution of [^{99m}Tc]**L2** in Tumor Bearing Mice[a]

	30 min	60 min
blood	0.28 ± 0.05	0.36 ± 0.11
heart	0.23 ± 0.01	0.22 ± 0.06
lung	0.82 ± 0.17	0.69 ± 0.14
liver	1.75 ± 0.40	1.15 ± 0.33
stomach	0.45 ± 0.12	0.36 ± 0.30
pancreas	0.35 ± 0.20	0.34 ± 0.16
spleen	10.36 ± 9.64	15.32 ± 6.64
kidney	47.86 ± 8.88	86.02 ± 13.93
muscle	0.54 ± 0.27	0.26 ± 0.11
small intestine	5.22 ± 1.92	2.35 ± 1.90
large intestine	1.25 ± 1.21	0.53 ± 0.42
bladder	0.46 ± 0.31	0.39 ± 0.18
PC-3 PIP	1.09 ± 0.61	2.04 ± 0.25
PC-3 flu	0.34 ± 0.18	0.46 ± 0.17
PIP:muscle	2	8
flu:muscle	0.6	2
PIP:flu	3	4

[a] Values in percent injected dose per gram ± standard deviation. $N = 4$ for all tissues.

Table 4. Biodistribution of [^{99m}Tc]**L3** in Tumor Bearing Mice[a]

	30 min	60 min	120 min	300 min
blood	0.68 ± 0.19	1.81 ± 1.61	0.08 ± 0.05	0.02 ± 0.00
heart	0.51 ± 0.13	1.56 ± 1.05	0.04 ± 0.01	0.04 ± 0.01
lung	2.48 ± 0.95	3.14 ± 1.82	0.13 ± 0.01	0.07 ± 0.00
liver	1.47 ± 0.14	2.85 ± 1.85	0.22 ± 0.05	0.17 ± 0.01
stomach	0.74 ± 0.15	3.87 ± 3.02	0.36 ± 0.19	0.12 ± 0.06
pancreas	0.61 ± 0.14	5.71 ± 4.68	0.12 ± 0.08	0.05 ± 0.00
spleen	32.07 ± 16.36	25.90 ± 10.08	0.98 ± 0.25	0.42 ± 0.07
fat	0.59 ± 0.17	4.67 ± 5.89	0.04 ± 0.01	0.02 ± 0.00
kidney	163.57 ± 29.62	178.56 ± 35.45	29.87 ± 27.09	1.91 ± 0.45
muscle	0.92 ± 0.25	1.42 ± 1.32	0.73 ± 0.25	0.04 ± 0.01
small intestine	10.62 ± 5.30	21.03 ± 4.46	0.58 ± 0.23	0.28 ± 0.20
large intestine	1.64 ± 0.71	6.49 ± 4.91	0.80 ± 0.40	0.53 ± 0.24
bladder	3.30 ± 1.06	10.38 ± 6.28	21.63 ± 35.22	0.43 ± 0.19
PC-3 PIP	11.56 ± 2.86	6.59 ± 5.22	1.89 ± 0.21	0.75 ± 0.55
PC-3 flu	0.53 ± 0.15	1.53 ± 1.69	0.32 ± 0.27	0.18 ± 0.17
PIP:muscle	13	5	3	18
flu:muscle	0.6	1	0.4	4
PIP:flu	23	4	6	4

[a] Values in percent injected dose per gram ± standard deviation. $N = 4$ for all tissues.

high and peaked at 95.66 ± 22.06%ID/g at 30 min and cleared to 1.26 ± 0.67%ID/g by 300 min pi.

Compound [^{99m}Tc]**L2** was also assayed for its pharmacokinetic characteristics in tumor-bearing mice, although only at 30 and 60 min pi. Table 3 shows the %ID/g of uptake for this radioligand. As for [^{99m}Tc]**L1**, [^{99m}Tc]**L2** showed PSMA-dependent tumor uptake, which peaked at 60 min pi at 2.04 ± 0.25%ID/g. That is significantly lower than the uptake observed for [^{99m}Tc]**L1** in the PC3 PIP tumor. The PIP:muscle ratios were also significantly lower, achieving a maximum value of only 7.7 at 60 min pi as opposed to a maximum of 41.4 for [^{99m}Tc]**L1** at 120 min pi. We speculate that the added lipophilicity of the bisquinoline moiety contributes to additional nonspecific binding (note relatively high liver uptake at 60 min pi (1.15 ± 0.33%ID/g for [^{99m}Tc]**L2** vs 0.25 ± 0.15%ID/g for [^{99m}Tc]**L1**) as well as the very high spleen uptake at that same time point (15.32 ± 6.64%ID/g)). Spleen had not yet reached equilibrium during the 60 min time course of this study. Kidney uptake at 60 min pi was 86.0 ± 13.9%ID/g, similar in value to that seen for [^{99m}Tc]**L1**.

The last compound to undergo detailed, ex vivo biodistribution assay, [^{99m}Tc]**L3**, also demonstrated PSMA-dependent tumor uptake, displaying highest PSMA+ PIP uptake at 30 min pi (11.56 ± 2.86% ID/g) (Table 4). PIP:flu ratios were highest at 30 min pi at 21.99 and then held steady at around 5:1 through 300 min pi. In this regard, both [^{99m}Tc]**L2** and [^{99m}Tc]**L3** are inferior in providing high PIP:flu ratios—the key criterion for PSMA-mediated imaging—as compared with [^{99m}Tc]**L1**. Compound [^{99m}Tc]**L3** exhibited a similar trend in liver, lung, and spleen as [^{99m}Tc]**L1** and [^{99m}Tc]**L2**. Radiotracer uptake within spleen and liver (nonspecific binding) were also very high for [^{99m}Tc]**L3**. PSMA-mediated kidney uptake was also similar to the other compounds of this class and peaked at 178.56 ± 35.45 at 60 min pi.

The remaining compounds of this series ([^{99m}Tc]**L4**−**L7**) underwent imaging (see below), however, the images suggested that these compounds did not warrant further ex vivo analysis.

Metabolism. Except for mouse kidney extracted 60 min after injection of [^{99m}Tc]**L1**, which contained 2% of its extracted radioactivity as a polar metabolite, all of the other tissue extracts, plasma, and urine at 30 and 60 min postinjection contained 100% of the chromatographed radioactivity as the parent compound.

Microscopy. Coordination of the bisquinoline moiety of **L2** with $Re(CO)_3$ renders this complex fluorescent. Accordingly, we performed microscopy using Re**L2** in live cells (Figure 2). Because the Stokes shift for Re**L2** is relatively large, it was necessary to excite at 494 nm and collect emission fluorescence at 628 nm. Efforts to excite at 321 nm, where the quantum efficiency for this ligand was expected to be highest, resulted in extreme autofluorescence and no useable data. Excitation in the green region of the spectrum, however, led to a weak but observable fluorescent signal from within the PSMA+ PC3 PIP cells. This result provides visual confirmation of internalization of low-molecular-weight ligands for PSMA. The mechanism of internalization of PSMA has been studied previously, however, only antibodies and antibody conjugates have been used rather than small molecules.[49,50]

Imaging. SPECT-CT imaging was carried out in SCID mice. Each mouse had a PSMA+ PC3 PIP and PSMA− PC3 flu xenograft in opposite, upper flanks. All radioligands were screened this way, and the results obtained were used to determine whether ex vivo biodistribution assay would add further information. Figure 3 shows early, rendered images of mice with radioligands that demonstrated positive PIP tumor uptake. Mice were injected intravenously with 0.5−1 mCi (19−37 MBq) of the corresponding ^{99m}Tc-labeled compound and were imaged at 45 min pi. Successful radioligands enabled visualization of both the PIP tumor and the kidneys, each of which expresses PSMA. Compounds [^{99m}Tc]**L1**−**L4** yielded positive scans with distinguishing features. Compound

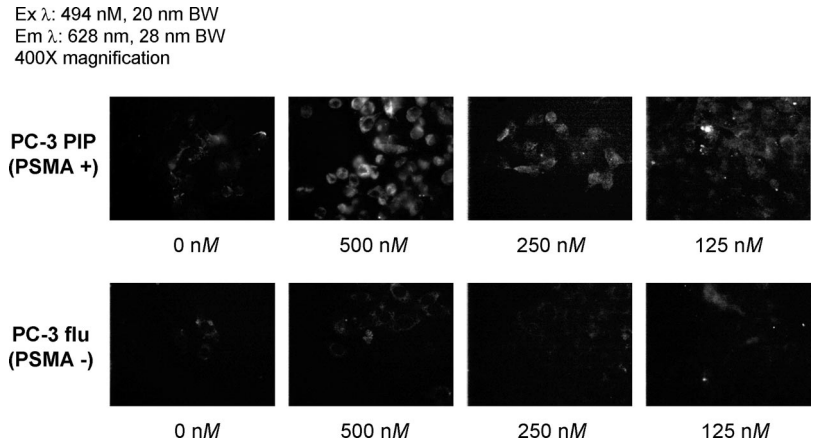

Figure 2. Fluorescence microscopy of PSMA+ PC-3 PIP cells and PSMA− PC-3 flu cells using Re**L2**.

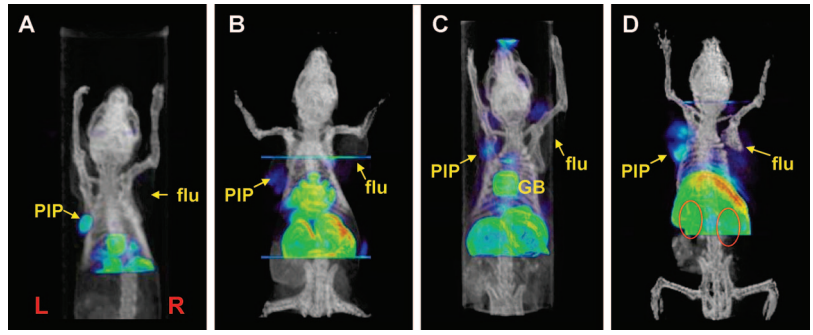

Figure 3. SPECT-CT imaging of tumor bearing mice with [^{99m}Tc]**L1**−**L4** (A−D, respectively). Dual pinhole SPECT-CT of PC-3 PIP and PC-3 flu tumor bearing mice. Mice were injected with 0.5−1 mCi (19−37 MBq) of radiopharmaceutical iv followed by a 45 min uptake period. Note essentially no uptake in the PSMA− flu tumors in each case. Abdominal radioactivity is primarily due to uptake within liver, spleen and kidneys. The horizontal lines in B are due to a reconstruction artifact at the boundaries of the field-of-view. PIP = PC-3 PIP; flu = PC-3 flu; GB = gallbladder in C; red circles highlight the location of the kidneys in D; L = left, R = right.

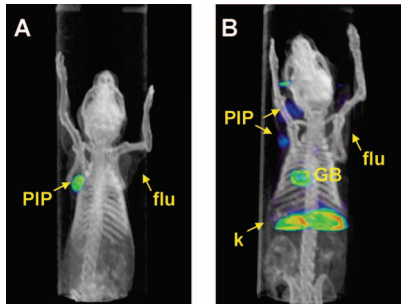

Figure 4. SPECT-CT imaging of tumor bearing mice with [^{99m}Tc]**L1** and [^{99m}Tc]**L3** (A and B, respectively). Dual pinhole SPECT-CT of PC-3 PIP and PC-3 flu tumor bearing mice. Mice were injected with 0.5−1 mCi (19−37 MBq) of radiopharmaceutical iv followed by a 3.5−4 h uptake period. Note lack of radiopharmaceutical outside of tumor in (A); however, the kidneys are outside of the field of view.

[^{99m}Tc]**L1** showed a strongly positive PIP tumor, gallbladder uptake, and clear visualization of the kidneys. Compound [^{99m}Tc]**L2** showed weak PIP tumor uptake, strong gallbladder uptake and kidney uptake. Compound [^{99m}Tc]**L3** showed strong PIP tumor uptake, despite the small size of the tumor, gallbladder uptake, and clear visualization of the kidneys. Compound [^{99m}Tc]**L4** showed elevated PIP tumor uptake as well as high liver and kidney uptake. Images obtained several hours after injection of [^{99m}Tc]**L1** or [^{99m}Tc]**L3** demonstrated higher contrast of tumor with respect to background (Figure 4), with very little radioactivity evident outside of the tumor for [^{99m}Tc]**L1**.

Compound [^{99m}Tc]**L5** produced images qualitatively similar to [^{99m}Tc]**L4**. Compounds [^{99m}Tc]**L6** and [^{99m}Tc]**L7** failed to show any PIP tumor uptake and instead showed only liver and kidney uptake (data not shown).

As a further test of in vivo binding specificity, we performed a blocking study using [^{99m}Tc]**L1** in an LNCaP (PSMA+) prostate tumor model but first pretreating the animal with 50 mg/kg of the potent, selective PSMA inhibitor, 2-(phosphonomethyl)pentanedioic acid (PMPA).[15,51] Figure 5 shows that PMPA is capable of eliminating binding of [^{99m}Tc]**L1** not only to tumor but also to the renal cortex, another site of specific binding for radiopharmaceuticals of this class. These results provide one more check on in vivo binding selectivity, using a blocking agent from a different chemical class than the urea-based inhibitors, and in a different, well-established, PSMA+ prostate tumor.

Discussion

Despite advances using a variety of imaging modalities, most notably MR spectroscopy, clinically viable molecular imaging of PCa has remained elusive. FDG-PET, which has worked so well not only for identification of primary and metastatic tumors but also for therapeutic monitoring, has largely failed in the case of PCa, perhaps due to the relatively low rate of metabolism of these tumors compared to other epithelial cancers. Although iterative reconstruction with anatomic coregistration can improve ProstaScint imaging[52] and using a radiolabeled version of the J591 human monoclonal antibody against an extracellular epitope of PSMA show some promise,[53,54] these agents will be fraught with the same disadvantages of all intact antibodies for

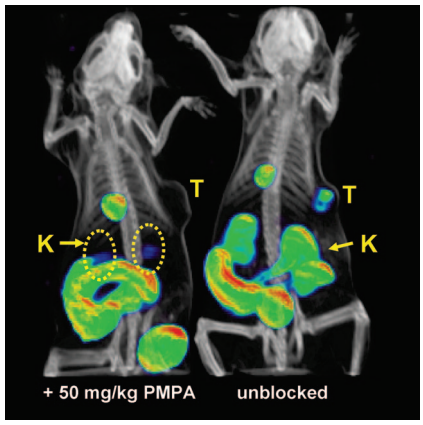

Figure 5. SPECT-CT imaging of LNCaP (PSMA+) tumor bearing mice with [^{99m}Tc]**L1** with (left) and without (right) blockade of PSMA using the potent, selective PSMA inhibitor, PMPA, as the blocking agent. Lack of radiopharmaceutical in both the tumor and kidneys (another PSMA+ site) upon cotreatment with PMPA provides a further check on PSMA-specific binding. Images were acquired from 30−60 min postinjection. T = tumor; K = kidney.

imaging, namely slow clearance from blood and nonspecific sites. Nevertheless, these antibodies bind to what we consider an ideal target for prostate cancer imaging and therapy— PSMA.

The radiopharmaceuticals we describe here are part of a series of new low-molecular-weight PSMA-based imaging agents. They are all based on ureas first described by Kozikowski et al., which are synthetically accessible, high-affinity inhibitors of PSMA.[55] We have previously demonstrated the specific binding of suitably functionalized ureas to PSMA for imaging with SPECT and PET. However, those agents were radiolabeled with either ^{125}I, ^{11}C, or ^{18}F.[13−15] Iodine-125-labeled agents can be used in conjunction with high-resolution small animal imaging devices to study experimental models and the isotope can be switched to ^{123}I or ^{124}I for human SPECT or PET, respectively. However, those isotopes are expensive ($1000/mCi for [^{124}I]NaI) and can be difficult to obtain on short notice. Carbon-11 is largely an experimental radionuclide for use only at centers that have a cyclotron in-house. Fluorine-18-labeled radiopharmaceuticals can be shipped limited distances, but those compounds will be of relatively low specific radioactivity upon arrival at the site of usage. Fluorine-18 also requires a cyclotron for production. For these reasons, the ready availability (via generators delivered to nuclear medicine departments daily) and ideal imaging characteristics of ^{99m}Tc, we have embarked on a program to synthesize ^{99m}Tc-labeled PSMA-based imaging agents. We have found that using SAAC technology developed by one of us (SRB)[56] in collaboration with Molecular Insight Pharmaceuticals, Inc. (Cambridge, MA), ^{99m}Tc can be readily incorporated in a sterically unobtrusive manner to these PSMA-binding ureas. Because Tc has no stable isotope, we used the group VIIB congener Re for the PSMA inhibitory studies.

We synthesized seven compounds, designated **L1**−**L7**, in both their Re- and ^{99m}Tc-labeled forms. All seven compounds derive from DCL (Chart 1), with different linkers between the ε amine of lysine and the chelator. Using SAAC technology, three different chelators were generated, namely the bispyridyl, the bisquinoline, and monopyridyl-monoacid. The primary rationale for the use of these different chelators was to exploit their differing degrees of steric bulk and lipophilicity. Both **L1** and **L2** provide cationic complexes upon complexation with the organometallic ^{99m}Tc(CO)$_3$/Re(CO)$_3$ core. On the other hand, **L4** offers a neutral complex for the metal tricarbonyl core. Compound **L2** provides the most lipophilic agent (Table 1). That degree of lipophilicity had a significant effect on both the in vitro binding as well as the in vivo imaging, with Re**L2** demonstrating 20-fold higher PSMA inhibitory activity than Re**L1**, but 6-fold lower PIP:flu at 1 h postinjection and significantly more liver and spleen uptake for the ^{99m}Tc analogue (Chart 2, Table 1, Figure 3). PIP and flu tumors are derived from PC3 human prostate cancer cells that differ only in their expression of PSMA (PIP = PSMA+, flu = PSMA−).[14,18] Another way to alter the lipophilicity of these complexes is to introduce a carboxylic acid moiety to various positions on the linker. Moving the linker carboxylic acid to the carbon adjacent to the chelator nitrogen caused the binding affinity to drop (Re**L3**) and provide lower PIP:flu and higher liver and spleen uptake than compound [^{99m}Tc]**L1** (Figure 3). In this series of three compounds, [^{99m}Tc]**L1** has the best properties for imaging in vivo despite its relatively low PSMA inhibitory potency.

Compounds Re**L4** and Re**L7** enable comparison of the bispyridyl and monopyridyl-monoacid chelators, respectively (Chart 2). Compound Re**L4** had a PSMA inhibitory potency of about 12-fold higher than that of Re**L7**. Although ex vivo biodistribution assays were not performed for these two compounds, [^{99m}Tc]**L4** demonstrated strong uptake in PIP as opposed to flu tumors, but there was also significant uptake within liver, an undesirable imaging characteristic perhaps due to the increased lipophilicity of this compound relative to [^{99m}Tc]**L1** and [^{99m}Tc]**L3**, which have a slightly shorter linker length and incorporate a linker acid moiety (Figure 3). Compound [^{99m}Tc]**L7** demonstrated no evidence of specific PIP tumor uptake and showed only radioactivity within the liver.

Compound **L5** has no amide or carboxylic acid within the linker and **L6** has the bispyridyl incorporated into the ε amine of lysine (Chart 2). The linker chain of **L5** is six carbons shorter than that of the **L1**−**L3** series. Compound Re**L6** demonstrated very low PSMA inhibitory activity, the lowest in the entire series, and [^{99m}Tc]**L6** showed no PIP tumor-specific uptake.

In this series, [^{99m}Tc]**L1** and Re**L2** have emerged as providing utility for imaging prostate cancer in vivo and in vitro, respectively. Compound [^{99m}Tc]**L1** is a promising clinical candidate because of its synthetic accessibility, very high target to nontarget ratio (PIP:flu = 44:1 at 2 h postinjection), rapid washout kinetics, metabolic stability, and the many salutary characteristics of ^{99m}Tc discussed above. The initial indication for its use would be to study patients who have undergone prostatectomy in whom a rising prostate-specific antigen (PSA) is detected—the same indication as for ProstaScint. Compound Re**L2** has documented the internalization of PSMA after binding of a low-molecular-weight agent to the active site (Figure 2). This compound could be used to study the kinetics of PSMA internalization. The internalization of compounds of this class suggests the development of the corresponding radiotherapeutic analogs. Future studies will involve further alterations in linker length and lipophilicity in an effort to binding to liver and other nonspecific sites.

Experimental Section

General Procedures. All reactions were performed under a nitrogen atmosphere unless otherwise noted. Solvents and chemicals obtained from commercial sources were of analytical grade or better and used without further purification. All experiments were performed in duplicate or triplicate to ensure reproducibility. Analytical thin-layer chromatography (TLC) was performed using Aldrich aluminum-backed 0.2 mm silica gel Z19, 329-1 plates and visualized by ultraviolet light (254 nm), I_2, and 1% ninhydrin in EtOH. Flash chromatography was performed using silica gel purchased from Bodman (Aston, PA), MP SiliTech 32−63 D 60

Å. In most cases, product isolation consisted of removing of the solvent from the reaction mixture, extracting with an organic solvent, washing with water and brine, drying with anhydrous sodium sulfate, filtering, and concentrating the filtrate. The use of such workup conditions will be indicated by the phrase "product isolation" (which is followed, in parentheses, by the extracting solvent). Purification in most cases was achieved by flash chromatography and is signified by the term "flash chromatography" (which is followed, in parentheses, by the elution solvent used). Melting points were measured using a Mel-Temp apparatus and are uncorrected. ^{1}H NMR spectra were recorded on either a Varian Mercury 400 MHz or on a Bruker Ultrashield 400 MHz spectrometer. Chemical shifts (δ) are reported in ppm downfield by reference to proton resonances resulting from incomplete deuteration of the NMR solvent. Low resolution ESI mass spectra were obtained on a Bruker Daltonics Esquire 3000 Plus spectrometer. Higher-resolution FAB mass spectra were obtained on a JEOL JMS-AX505HA mass spectrometer in the mass spectrometer facility at the University of Notre Dame. Optical rotation was measured on a Jasco P-1010 polarimeter. Infrared spectra were obtained on a Bruker Tensor 27 spectrometer. High-performance liquid chromatography (HPLC) purification of **L1**−**L7** and Re**L1**−Re**L7** using a Phenomenex C_{18} Luna 10 × 250 mm^2 column was performed on a Waters 600E Delta LC system with a Waters 486 tunable absorbance UV/vis detector, both controlled by Empower software. Purification of Re**L1**−**L7** and [^{99m}Tc]**L1**−**L7** by HPLC was performed using the following isocratic conditions: method 1, the mobile phase was 65% solvent A (0.1% TFA in water) and 35% solvent B (0.1% TFA in CH_3CN), flow rate 2 mL/min; method 2, mobile phase was 65% solvent A and 35% solvent B, flow rate 4 mL/min; method 3, mobile phase was 70% solvent A and 30% solvent B, flow rate 2 mL/min. Eluant was monitored at 254 and 220 nm. For radiosynthetic purification, HPLC was performed with a Waters Chromatography Division HPLC system equipped with two model 510EF pumps, a model 680 automated gradient controller, a model 490 UV absorbance detector, and a Bioscan NaI scintillation detector connected to a Bioscan Flow-count system. The output from the UV detector and the Flow-count radiodetector system were fed into a Gateway 2000 P5-133 computer fitted with an IN/US System, Inc. computer card and analyzed using Winflow software (IN/US). Absorption spectra were collected using a Hewlett-Packard 8453 spectrophotometer. The Isolink kit was a generous gift from Mallinckrodt-Tyco Health Care (St. Louis, MO, USA).

2-Amino-6-*tert*-butoxycarbonylamino-hexanoic acid 4-methoxybenzyl ester (2). Compound **2** was prepared in two steps. Into a 250 mL, flame-dried three-necked round-bottom flask under nitrogen was placed N_ε-Boc-N_α-Fmoc-L-lysine (7.0 g, 15 mmol) and 60 mL of dry DMF. To this was added cesium carbonate (7 g, 21 mmol) and 4-methoxybenzyl chloride (2.5 g, 16 mmol). The suspension was stirred at room temperature under nitrogen for 4 h, then filtered and washed with ethyl acetate. Product isolation (EtOAc, 5% Na_2CO_3, water, Na_2SO_4) followed by recrystallization from 60/40 (v/v) hexane/EtOAc gave 2 crops of a colorless solid. mp 118−120 °C. TLC R_f = 0.33 (70/30 hexane/EtOAc). Yield: 8.22 g, 14 mmol, 93.43%. ^{1}H NMR($CDCl_3$) δ: 7.75 (d, J = 7.2 Hz, 2H), 7.55 (d, J = 7.2 Hz, 2H), 7.38 (t, J = 7.5 Hz, 2H), 7.32−7.20 (m, 4H), 6.85−6.80 (m, 2H), 5.4 (d, J = 7.6 Hz, 1H), 5.18−5.00 (m, 2H), 4.44−4.38 (m, 3H), 4.17 (t, J = 6.0 Hz 1H), 3.80−3.70 (m, 4H), 3.00 (m, 2H), 1.90−1.11 (m, 15H). ESIMS m/z: 588.40 [M + 1]$^+$. Into a flame-dried round-bottom flask was placed 5.0 g (8.54 mmol) of the fully protected analogue of **2**. This was dissolved in 60 mL of a 20% solution of piperidine in DMF. The reaction was stirred at room temperature for 2 h. Product isolation (CH_2Cl_2, water, Na_2SO_4) followed by flash chromatography (4/96 MeOH/$CHCl_3$) afforded a pure **2** as an oil (2.59 g, 7.07 mmol) in 83% yield. (TLC R_f = 0.42 in 5/95 MeOH/CH_2Cl_2). ^{1}H NMR ($CDCl_3$) δ: 7.29 (d, J = 7.2 Hz, 2H), 6.90 (d, J = 7.2 Hz, 2H), 5.09 (m, 2H), 4.44−4.24 (m, 1H), 3.83 (s, 3H), 2.76−58 (m, 3H), 2.11−1.34 (m, 16H). ESIMS m/z: 367[M + 1]$^+$ for $C_{19}H_{31}N_2O_5$.

2-{3-[1-*p*-Methoxybenzylcarboxylate-(5-*t*-butylcarbamylpentyl)]-ureido}-di-*p*-methoxybenzyl pentanedioate (3). Bis-4-methoxybenzyl-L-glutamate·HCl **4** (3.6 g, 8.5mmol)[31,32] was placed in a flame-dried three-neck round-bottom flask under nitrogen and dissolved in 15 mL CH_2Cl_2. Triphosgene (0.833 g, 2.8 mmol) was placed in a vial, dissolved in 3 mL CH_2Cl_2 and added to the three neck flask. The flask was cooled to −77 °C (dry ice ethanol slurry) under nitrogen. To this was slowly added triethylamine (12 mL, 85 mmol in 10 mL CH_2Cl_2). The reaction mixture was stirred at −77 °C for 1 h, allowed to warm to room temperature and was stirred for 30 min at rt. To this was added compound **2** (3.1 g, 8.5 mmol in 7 mL CH_2Cl_2). The resulting mixture was stirred overnight. Product isolation (CH_2Cl_2, water, NaCl, Na_2SO_4) followed by flash chromatography (20/80 EtOAc/CH_2Cl_2) afforded an oil that solidified upon standing. Yield: 4.135 g, 5.3 mmol, 62.3%. TLC R_f = 0.47 (20/80 EtOAc/CH_2Cl_2). ^{1}H NMR ($CDCl_3$) δ: 7.26−7.2 (m, 6H), 6.86−6.80 (m, 6H), 5.89 (m, 2H), 5.12−5.0 (m, 6H), 4.51 (m, 1H), 4.45 (m, 1H), 3.77 (s, 9H), 2.98 (m, 2H), 2.36 (m, 2H), 2.12 (m, 1H), 1.92 (m, 1H), 1.70 (m, 1H), 1.58 (m, 1H), 1.4 (m, 11H), 1.24 (m, 3H). ESIMS m/z: 780 [M + 1]$^+$. HRFAB$^+$-MS: calcd for $C_{41}H_{54}N_3O_{12}$, 780.3679, [M + 1]$^+$, observed 780.3685 [M + 1]$^+$. $^{25}[\alpha]_D$ = −3.440 (0.12, DMF).

***p*-Toluenesulfonate salt of 2-{3-[1-*p*-methoxybenzylcarboxylate-(5-aminopentyl)]-ureido}-di-*p*-methoxybenzyl pentanedioate (5).** A solution of **3** (2 g, 2.6 mmol) dissolved in 20 mL EtOAc was cooled to 0−2 °C in an ice bath and *p*-toluenesulfonic acid monohydrate (0.49 g, 2.6 mmol) in 5 mL of absolute ethanol was added. The cooling bath was removed, and the reaction mixture was allowed to warm to room temperature for 2 h. The reaction mixture was then concentrated to a thick oil under reduced pressure, and the mixture was purified with flash chromatography using 10/90 MeOH/CH_2Cl_2 to afford product as colorless solid in 45% (0.98 g, 1.15mmol) yield. TLC R_f = 0.47 (10/90 MeOH/CH_2Cl_2). ^{1}H NMR ($CDCl_3$): δ 7.68 (d, J = 8.0 Hz, 2H), 7.66−7.57 (s, broad, 3H), 7.22−7.13 (m, 6H), 7.0 (d, J = 7.2 Hz, 2H), 6.84−6.76 (m, 6H), 6.34 (s broad, 2H), 5.06−4.88 (m, 6H), 4.44 (m, 1H), 4.32 (m, 1H), 3.76 (s, 3H), 3.73 (s, 6H), 2.86 (s, broad, 2H), 2.3−2.24 (singlet on top of multiplet, 5H), 2.08−1.99 (m, 1H), 1.82−1.72 (m, 1H), 1.64−1.3 (m, 6H). ESIMS m/z: 680 [M$^+$ + 1]. HRFAB$^+$-MS: calcd for $C_{36}H_{46}N_3O_{10}$, 680.3178 [M$^+$]; found, 680.3177.

2-{3-[1-*p*-Methoxybenzylcarboxylate-(5-aminopentyl)]-ureido}-di-*p*-methoxybenzyl pentanedioate (1). A solution of **5** (0.15 g, 0.17 mmol in 50 mL CH_2Cl_2) was placed in a separatory funnel, washed with 100 mL of 0.5 M $NaHCO_3$. The organic layer was collected, dried over anhydrous Na_2SO_4, filtered, and concentrated to a yellow film (0.107 g, 0.09 mmol, 52.5%). TLC R_f = 0.40 (10/90 MeOH/CH_2Cl_2). ^{1}H NMR ($CDCl_3$): δ 7.2−7.12 (m, 6H), 6.8−6.72 (m, 6H), 5.84 (s broad, 2H), 5.04−4.90 (m, 6H), 4.44−4.34 (m, 2H), 3.7 (m, 9H), 2.6 (s broad, 2H), 2.3 (m, 2H), 2.06 (m, 1H), 1.85 (m, 1H), 1.66 (m, 1H), 1.55 (m, 1H), 1.44−1.12 (m, 4H). ESIMS: 680 [M + 1]$^+$. Compound **1** was used immediately in the next step.

2-{3-[5-[7-(2,5-Dioxo-pyrrolidin-1-yloxycarbonyl)-heptanoylamino]-1-(4-methoxy-benzyloxycarbonyl)-pentyl]-ureido}-pentanedioic Acid Bis-(4-methoxy-benzyl) Ester (6). A 100 mL round-bottom flask was flame-dried under N_2, after which **1** (0.08 g, 0.12 mmol) was added and then dissolved in 10 mL of dry DMF. This solution was added dropwise to a solution of suberic acid bis-(*N*-hydroxysuccinimide ester), DSS (0.13 g, 0.35 mmol in 10 mL DMF), at room temperature with mild stirring. After 2 h, the volume of the solution was reduced under vacuum, and the colorless solid residue was kept under high vacuum for 2 h further to remove traces of DMF. The residue was dissolved in 1 mL of CH_2Cl_2 and was loaded onto silica gel column (1 in. × 12 in.). Initially, the column was eluted with 40/60 CH_3CN/CH_2Cl_2 to remove excess DSS followed by 50/50 CH_3CN/CH_2Cl_2 to afford the product as a colorless solid. Yield: 0.062 mg, 0.07 mmol, 56.6%. TLC R_f = 0.47 (5/95 MeOH/CH_2Cl_2). ^{1}H NMR($CDCl_3$): δ 7.26 (m, 6H), 6.86 (m, 6H), 5.91 (m, 1H), 5.37 (m, 4H), 5.03 (m, 6H), 4.43 (m, 3H), 3.79 (s, 9H), 3.31 (m, 4H), 2.82 (s, 4H), 2.58 (t, J = 8.4 Hz, 2H), 2.37 (m, 2H), 2.14 (m,

4H), 1.71−1.21 (m, 9H). ESIMS *m/z*: 933 [M + 1]. (HRFAB$^+$-MS): calcd for $C_{48}H_{61}N_4O_{15}$ [M + 1]$^+$, 933.4133; found, 933.4142 [M + 1]$^+$.

Compounds **L1**−**L3** were prepared by following the same general synthetic procedure as shown in Scheme 2 for **L1** as a representative case.

2-[3-(5-{7-[5-(Bis-pyridin-2-ylmethyl-amino)-1-carboxy-pentyl-carbamoyl]-heptanoylamino}-1-carboxy-pentyl)-ureido]-pentanedioic Acid (L1). A solution of **7**[35] (0.035 g, 0.107 mmol in 0.5 mL MeOH) was added to a stirred solution of **6** (0.100 g, 0.107 mmol in 6 mL dry DMF) at room temperature followed by the addition of 0.2 mL NEt_3. The reaction mixture was stirred for 10 h at room temperature. The reaction mixture was then concentrated under reduced pressure. Product isolation (CH_2Cl_2, water, Na_2SO_4) followed by flash chromatography (50/50 MeOH/CH_2Cl_2) afforded the intermediate compound as a colorless solid in 74% yield (0.090 g, 0.08 mmol). TLC R_f = 0.45 (40/60 MeOH/CH_2Cl_2). ESIMS *m/z*: 1146.7 [M + 1]$^+$, 1168.7 [M + Na]$^+$. The above intermediate compound (20 mg, 0.017 mmol) was dissolved in an ice-cold solution of TFA (7 mL) and anisole (0.3 mL) and was stirred for 10 min. The ice bath was removed and the solution was allowed to warm to room temperature with continued stirring for another 10 min. The solution was evaporated under reduced pressure, and the light-brown residue was dried under high vacuum for 2 h. The residue was washed with diethyl ether (3 × 5 mL) and water (10 × 2 mL) to produce crude **L1**. Yield: 9 mg, 0.011 mmol, 65%. The colorless product was dried under vacuum and purified further by HPLC using 75/25 water (0.1% TFA)/acetonitrile (0.1%TFA) as mobile phase, flow rate 2 mL/min; R_t = 14 min. ^{1}H NMR (D_2O): δ 8.71 (d, J = 5.6 Hz, 2H), 8.52 (t, J = 8 Hz, 2H), 8.05 (d, J = 8 Hz, 2H), 7.96 (t, J = 6.8 Hz, 2H), 4.32−4.18 (m, 7H), 3.80−3.70 (m, 1H), 3.18 (t, J = 6 Hz, 2H), 2.69 (m, 2H), 2.51 (t, J = 7.6 Hz, 2H), 2.40−2.18 (m, 25H). ^{13}C NMR (D_2O): δ 177.2, 177.13, 163.10, 162.8, 159.2, 152.4, 146.1, 142.3, 126.8, 126.1, 55.8, 54.4, 46.6, 38.8, 35.6, 35.2, 30.6, 30.0, 29.9, 27.7, 27.6, 26.3, 25.2, 25.0, 24.3, 22.4, 22.3. ESIMS *m/z*: 786 [M + 1]. HRFAB$^+$-MS: calcd for $C_{38}H_{56}N_7O_{11}$ [M + 1], 786.4038; found, 786.4033.

2-[3-(5-{7-[5-(Bis-quinolin-2-ylmethyl-amino)-1-carboxy-pentyl-carbamoyl]-heptanoylamino}-1-carboxy-pentyl)-ureido]-pentanedioic acid (L2). Compound **L2** was obtained by reacting compound **8**[39] with compound **6** similarly as described above for **L1**. HPLC purification was done by using 70/30 water (0.1% TFA)/CH_3CN (0.1% TFA) as mobile phase, flow rate 4 mL/min; R_t = 9 min. ^{1}H NMR(D_2O/CD_3CN 2/1): δ 8.81 (d, J = 8.0 Hz, 2H), 8.42 (d, J = 8.4 Hz, 2H), 8.33 (d, J = 8.4 Hz, 2H), 8.22 (t, J = 7.6 Hz, 2H), 8.05 (t, J = 7.8 Hz, 2H), 7.97 (d, J = 8.4 Hz, 2H), 5.11 (s, 4H), 4.66−4.64 (m, 1H), 4.57−4.54 (m, 1H), 4.47−4.46 (m, 1H), 3.71 (m, 2H), 3.51−3.43 (m, 3H), 2.77 (t, J = 7.6 Hz, 2H), 2.51 (m, 3H) 2.20−1.5 (m, 26H). ESIMS *m/z*: 902 [M + H_2O]. HRFAB$^+$-MS: $C_{46}H_{60}N_7O_{12}$ [M + H_2O], 902.4300; found, 902.4290.

2-[3-(5-{7-[5-(Bis-pyridin-2-ylmethyl-amino)-5-carboxy-pentyl-carbamoyl]-heptanoylamino}-1-carboxy-pentyl)-ureido]-pentanedioic acid (L3). Compound **L3** was prepared by reacting compound **9**[35] with compound **6** similarly as described above for **L1.** HPLC purification was done by using 75/25 water (0.1% TFA)/CH_3CN (0.1% TFA) as mobile phase, flow rate 2 mL/min, R_t = 8 min. ^{1}H NMR (D_2O): δ 8.68 (d, J = 6.0 Hz, 2H), 8.50 (t, J = 7.6 Hz, 2H), 8.06 (d, J = 5.6 Hz, J = 7.9 Hz, 2H), 7.94 (t, J = 6.4 Hz, 2H), 4.32−4.37 (m, 4H), 4.25 (m, 1H), 4.18 (m, 1H), 3.48 (t, J = 7.2 Hz, 1H), 3.16 (m, 2H), 2.69 (m, 2H), 2.48 (t, J = 7.2 Hz, 2H), 2.18−2.15 (m, 5H), 1.97−1.20 (m, 21H). ESIMS *m/z*: 786 [M + 1]$^+$. HRFAB$^+$-MS: calcd for $C_{38}H_{55}N_7O_{11}$, 786.4038 [M + 1]; found, 786.4032.

2-[3-(1-Carboxy-5-{7-[6-(carboxymethyl-pyridin-2-ylmethyl-amino)-hexylcarbamoyl]-heptanoylamino}-pentyl)-ureido]-pentanedioic acid (L4). Compound **10** was prepared following a published procedure.[36] Compound **11** was prepared as follows: to a solution of compound **10** (0.517 g, 1.7 mmol) in 10 mL of CH_2Cl_2 was added a solution of glyoxylic acid monohydrate (1.55 g, 1.68 mmol in 1 mL of MeOH containing activated molecular sieves) and was stirred for 30 min. Sodium triacetoxyborohydride (0.712 g, 3.3 mmol) was added to the solution in small portions and stirred overnight at ambient temperature. Product isolation (CH_2Cl_2, water, NaCl, Na_2SO_4) afforded crude compound that was used in the next step without further purification. Yield: 0.483 g, 1.32 mmol, 78.6%. TLC R_f =0.37 (10/90 MeOH/CH_2Cl_2). ^{1}H NMR ($CDCl_3$): δ 8.62 (m, 1H), 7.75 (m, 1H), 7.32 (m, 2H), 4.56 (bs, 1H), 4.04 (s, 2H), 3.46 (s, 2H), 3.14 (m, 2H), 2.78 (m, 2H), 2.09 (m,1H), 1.74−1.16 (m, 16H). ESIMS *m/z*: 366.7 [M + 1], 388.5 [M + Na].The removal of t-Boc was performed by dissolving the crude compound (0.483 g, 1.32 mmol) in an ice-cold solution of 10 mL 1/1 TFA/CH_2Cl_2. The reaction mixture was allowed to stir at room temperature for 4 h. The solution was evaporated under reduced pressure and dried under vacuum to provide a colorless solid of **11** and was used without further purification. Yield: 0.315 g, 1.19 mmol, 90%. ^{1}H NMR (MeOH-d_4): δ 8.52 (d, J = 5.6 Hz 1H), 7.78 (t, J = 7.6 Hz, 1H), 7.54 (d, J = 7.4 Hz, 1H), 7.29 (t, J = 7.2 Hz, 1H), 3.78 (s, 2H), 3.22 (s, 2H), 2.85 (t, J = 8.0 Hz, 2H), 2.5 (t, 2H), 1.72−1.20 (m, 8H). ESIMS *m/z*: 266.3 [M + 1]$^+$, 288.3 [M + Na]$^+$. Compound **L4** was prepared by coupling compound **6** with compound **11**. Compound **L4** was purified by HPLC using 76/24 water (0.1% TFA)/CH_3CN (0.1% TFA) as the mobile phase, flow rate: 2 mL/min, R_t = 10.2 min. ^{1}H NMR (D_2O): δ 8.62 (d, J = 5.6 Hz, 1H), 8.15 (t, J = 6.4 Hz,1H), 7.95 (d, J = 7.6 Hz, 1H), 7.88 (t, J = 6.4 Hz, 1H), 4.25 (m, 1H), 4.23−4.1 (m, 2H), 3.35 (m, 2H), 3.25−3.31 (m, 5H), 2.84 (m, 1H), 2.52 (t, J = 6.8 Hz, 2H,) 2.27 (m, 6H), 1.64−1.21 (m, 23H). ESIMS *m/z*: 723 [M + 1]$^+$and 745.7 for [M + Na]$^+$. HRFAB$^+$-MS: calcd for $C_{35}H_{55}N_6O_{11}$, 723.3929 [M + 1]; found, 723.3912.

2-(3-{5-[8-(Bis-pyridin-2-ylmethyl-amino)-octanoylamino]-1-carboxy-pentyl}-ureido)-pentanedioic Acid (L5). To a solution of 8-(bis-pyridin-2-ylmethyl-amino)-octanoic acid[35] (0.9 g, 2.6 mmol, 15 mL DMF) was added *O*-benzotriazol-1-yl-*N*, *N*, *N*′, *N*′-tetramethyluronium hexafluorophosphate (1.49 g, 3.9 mmol) and *N*-hydroxysuccinimide (0.36 g, 3.1 mmol). The reaction mixture was stirred at room temperature for 16 h. After removing solvent under reduced pressure, the crude product was purified by flash chromatography (10/90 MeOH /CH_2Cl_2) to give **12** as a thick, colorless liquid. Yield: 0.75 g, 0.17 mmol, 65%. ^{1}H NMR ($CDCl_3$): δ 8.58 (d, J = 4.8 Hz, 2H), 7.78 (t, J = 8.0 Hz, 2H), 7.50 (d, J = 7.6 Hz, 2H), 7.32 (t, J = 8.0 Hz, 2H), 4.62 (s, 4H), 3.27 (t, J = 7.6 Hz, 2H), 2.82 (s, 4H), 2.58 (d, J = 7.2 Hz, 2H), 1.82−1.66 (m, 4H), 1.33−1.28(m, 6H). ESIMS: 439 [M + 1]$^+$. To a solution of **12** (0.052 g, 0.11 mmol in 7 mL CH_2Cl_2) was added **5** (0.1 g, 0.11 mmol), followed by NEt_3 (0.2 mL, 1.4 mmol). The reaction mixture was stirred at room temperature for 5 h and then concentrated under reduced pressure. Product isolation (EtOAc, water, NaCl, Na_2SO_4) followed by flash chromatography (50/50 MeOH/CH_2Cl_2) afforded pure compound the 4-methoxybenzyl ester of **L5** in 51% (0.060 g, 0.056 mmol) yield. Cleavage of the PMB groups by stirring for 2 h in 1/1 TFA/CH_2Cl_2 followed by removal of solvent gave a solid residue. The residue was dissolved in 7 mL water, washed with 3 × 10 mL CH_2Cl_2 and the water layer concentrated under vacuum to provide crude **L5**. The compound was further purified by HPLC with 80/20 water (0.1% TFA)/CH_3CN (0.1% TFA) solution as the mobile phase. The flow rate was 3 mL/min, R_t = 8 min. ^{1}H NMR (D_2O): δ 8.74 (d, J = 6.0 Hz, 2H); 8.52 (t, J = 8.0 Hz, 2H), 8.04 (d, J = 8.0 Hz, 2H), 7.95 (t, J = 6.4 Hz, 2H), 4.32 (s, 4H), 4.23 (s, 1H), 4.14 (s, 1H), 3.24 (t, J = 6.4 Hz, 2H), 2.67 (t, J = 7.6 Hz, 2H), 2.49 (t, J = 7.2 Hz, 2H), 2.16 (m, 3H), 1.95 (m, 1H), 1.79 (m, 1H), 1.68 (m, 1H), 1.6−1.0 (m, 14H). ESIMS *m/z*: 643 [M + 1]$^+$. HRFAB$^+$-MS: calcd for $C_{32}H_{47}N_6O_8$, 643.3455 [M + 1]; found 643.3463.

2-{3-[5-(Bis-pyridin-2-ylmethyl-amino)-1-carboxy-pentyl]-ureido}-pentanedioic acid (L6). To a solution of pyridine-2-aldehyde (50 mg, 0.44 mmol in 4 mL CH_2Cl_2) was added a solution of **1** (100 mg, 0.147 mmol in 4 mL CH_2Cl_2). This was stirred at ambient temperature for 2 h. The reaction mixture was cooled to 0 °C, and sodium triacetoxyborohydride (93 mg, 0.44 mmol) was then added with stirring for an additional 3 h while warming to ambient temperature. Product isolation (CH_2Cl_2, water, NaCl, Na_2SO_4) followed by flash chromatography (10/90 MeOH/CH_2Cl_2) afforded

a colorless solid as the tri-PMB ester of **L6**. Removal of the PMB groups was effected by dissolving in 5 mL of 50/50 TFA/CH_2Cl_2 and was stirred at room temperature for 2 h. The resulting solution was concentrated to provide a colorless solid. The solid was dissolved in 3 mL water and washed with 5 × 5 mL CH_2Cl_2. The water layer was concentrated to provide a solid. Yield: 132 mg, 0.26 mmol, 61%. The product was purified by HPLC using 85/15 water (0.1% TFA)/CH_3CN (0.1% TFA) solution as mobile phase. Flow rate was 3 mL/min, R_t =13 min. ^{1}H NMR (D_2O): δ 8.78 (d, J = 5.2 Hz, 2H), 7.89 (t, J = 7.7 Hz, 2H), 7.49 (d, J = 7.6 Hz, 2H), 7.34 (t, J = 6.4 Hz, 2H), 4.75−4.62 (m, 4H), 4.45−4.22 (m, 2H), 2.75 (m, 2H), 2.55 (t, J = 6.6 Hz, 2H), 2.2−1.01 (m, 7H). ESIMS: 502 $[M + 1]^+$. HRFAB$^+$: for $C_{24}H_{31}N_5O_7$ calcd, 501.2224; found, 502.2296.

2-[3-(5-{7-[6-(Bis-pyridin-2-ylmethyl-amino)-hexylcarbamoyl]-heptanoylamino}-1-carboxy-pentyl)-ureido]-pentanedioic acid (L7). Compound **L7** was prepared by reacting **13**[35] with **6** similarly as described above for **L1**. HPLC purification was performed using 75/25 water (0.1% TFA)/CH_3CN (0.1% TFA) as mobile phase, flow rate 3 mL/min, R_t= 5.5 min. ^{1}H NMR (D_2O): δ 8.65 (d, J = 5.2 Hz, 2H), 7.99 (t, J = 8.6 Hz, 2H), 7.59−7.54 (m, 4H), 4.59 (s, 4H), 4.21−4.14 (m, 2H), 3.29−3.17 (m, 7H), 2.48 (t, J = 7.6 Hz, 2H), 2.27−2.22 (m, 6H), 1.82−1.32 (m,19H). ESIMS *m/z*: 756 $[M+1]^+$. HRFAB$^+$-MS: calcd for $C_{38}H_{55}N_7O_{11}$, 756.4296 [M + 1]; found, 756.4032.

All rhenium compounds were synthesized as for **ReL1**, for which a detailed example is provided below.

Tricarbonyl (2-[3-(5-{7-[5-(bis-pyridin-2-ylmethyl-amino)-1-carboxy-pentylcarbamoyl]-heptanoylamino}-1-carboxy-pentyl)-ureido]-pentanedioic acid) rhenium bromide (ReL1). Compound **L1** (0.058 g, 0.074 mmol) was dissolved in 10 mL of water. A solution of $[Re(CO)_3(H_2O)_3]Br$[37] (0.029 mg in 0.5 mL methanol) was added and the reaction mixture was refluxed for 4 h. The solution was concentrated to provide a colorless solid that was washed with 3 × 10 mL diethyl ether, 3 × 10 mL CH_2Cl_2, and finally with water. Products were dried under vacuum and purified by HPLC method 1. R_t = 12 min. ^{1}H NMR (5/1 D_2O/CH_3CN): δ 9.31 (d, J = 5.4 Hz, 2H,), 8.64 (t, J = 8 Hz, 2H), 7.88 (d, J = 8 Hz, 2H), 7.85 (t, J = 8 Hz, 2H,), 5.25−5.18 (m, 4H), 4.26 (m, 2H), 3.61 (t, J = 5.2 Hz, 2H), 2.75 (t, J = 6.4 Hz, 2H), 2.66 (t, J = 7.2 Hz, 2H), 2.55−2.45 (m, 27H). ESIMS *m/z*: 1056 $[M^+]$. HRFAB$^+$-MS: calcd for $C_{41}H_{55}N_7O_{14}Re$ $[M^+]$, 1056.3364; found, 1056.3350 $[M^+]$. IR ν (cm^{-1}) $[Re(CO)_3]^+$: 2030, 1912.

Tricarbonyl(2-[3-(5-{7-[5-(bis-quinolin-2-ylmethyl-amino)-1-carboxy-pentylcarbamoyl]-heptanoylamino}-1-carboxy-pentyl)-ureido]-pentanedioic acid) rhenium bromide (ReL2). For HPLC purification, method 2 was used. R_t = 16 min. ^{1}H NMR (1/1 D_2O/CD_3CN): δ 8.81−8.74 (m, 4H), 8.30 (d, J = 8.0 Hz, 2H), 8.16 (t, J = 8.0 Hz, 2H), 7.99 (t, J = 7.2 Hz, 2H), 7.90 (d, J = 8.0 Hz, 2H), 5.42−5.37 (m, 2H), 5.38−5.22 (m, 2H), 4.68−4.64 (m, 1H), 4.53−4.51 (m, 1H), 4.45−4.42 (m, 1H), 4.06−4.04 (m, 2H), 3.37 (t, J = 6.8 Hz, 2H), 2.72 (t, J = 7.2 Hz, 2H), 2.51 (t, J = 7.2 Hz, 2H), 2.40−1.30 (bm, 24H). ESIMS *m/z*: 1156 $[M]^+$. HRFAB$^+$-MS: calcd for $C_{49}H_{59}N_7O_{14}Re$ $[M]^+$, 1156.3677; found, 1156.3662 $[M^+]$. IR ν(cm^{-1}) $[Re(CO)_3]^+$: 2028, 1900.

Tricarbonyl(2-[3-(5-{7-[5-(bis-pyridin-2-ylmethyl-amino)-5-carboxy-pentylcarbamoyl]-heptanoylamino}-1-carboxy-pentyl)-ureido]-pentanedioic acid)rehenium bromide (ReL3). For HPLC purification method 3 was used. Flow rate was 2 mL/min, R_t = 11.5 min. ^{1}H NMR (5/1 D_2O/CH_3CN): δ 9.26 (d, J = 5.6 Hz, 1H), 9.20 (d, J = 5.6 Hz, 1H), 8.36 (t, J = 8.0 Hz, 2H), 7.90 (m, 2H), 7.83 (m, 2H), 5.31−5.03 (m, 4H), 3.67 (t, J = 6.8 Hz, 2H), 3.53 (t, J = 6.6 Hz, 2H), 3.15 (t, 2H), 2.40−1.30 (bm, 29H). ESIMS *m/z*: 1056 $[M]^+$. HRFAB$^+$-MS: calcd for $C_{41}H_{55}N_7O_{14}Re$ $[M]^+$, 1056.3364; found, 1056.3350 $[M^+]$.

Tricarbonyl(2-[3-(1-carboxy-5-{7-[6-(carboxymethyl-pyridin-2-ylmethyl-amino)-hexylcarbamoyl]-heptanoylamino}-pentyl)-ureido]-pentanedioic acid) rhenium (ReL4). For HPLC purification, method 1 was used. R_t = 18 min. (D_2O:CH_3CN(5:1)): δ 9.29 (d, J = 5.6 Hz, 1H), 9.22 (d, J = 8.0 Hz, 1H), 8.88 (d, J = 8.0 Hz, 1H), 7.84 (t, J = 8.0 Hz, 1H), 5.31−5.03 (m, 2H), 4.67 (m, 2H), 4.25 (m, 2H), 3.53 (m, 2H), 3.35 (t, J = 7.8 Hz, 2H), 2.72 (m, 2H), 2.46−1.30 (bm, 30H). ESIMS *m/z*: 993 $[M + 1]^+$. HRFAB$^+$-MS: calcd for $C_{37}H_{54}N_6O_{14}Re$ 993.3255 $[M + 1]^+$; found, 993.3237.

Tricarbonyl(2-(3-{5-[8-(bis-pyridin-2-ylmethyl-amino)-octanoylamino]-1-carboxy-pentyl}-ureido)-pentanedioic acid)rhenium bromide (ReL5). For HPLC purification, method 1 was used. R_t = 17 min. ^{1}H NMR (5/1 D_2O/CH_3CN): δ 9.23 (d, J = 5.6 Hz, 2H), 8.34 (t, J = 8.0 Hz, 2H), 7.72 (d, J = 8 Hz, 2H), 7.77 (t, J = 6.4 Hz, 2H), 5.13 (m, 4H), 4.66 (m, 1H), 4.58 (m, 1H), 4.16 (m, 2H), 3.56 (t, J = 6.8 Hz, 2H), 2.86 (t, J = 7.6 Hz, 2H), 2.59−1.6 (m, 20H). ESIMS *m/z*: 913 $[M]^+$. HRFAB$^+$-MS: calcd for $C_{35}H_{46}N_6O_{11}Re$, $[M]^+$ 914.2860; found, 914.2833.

Tricarbonyl(2-{3-[5-(bis-pyridin-2-ylmethyl-amino)-1-carboxy-pentyl]-ureido}-pentanedioic acid)rhenium bromide (ReL6). For HPLC purification, method 1 was used. R_t = 10.1 min. ^{1}H NMR (CD_3CN): δ 9.12 (d, J = 5.6 Hz, 2H), 8.22 (t, J = 7.7 Hz, 2H), 7.80 (d, J = 8.0 Hz, 2H), 7.65 (t, J = 6.5 Hz, 2H), 5.03 (m, 4H), 4.59−4.58 (m, 2H), 4.08 (m, 2H), 2.79 (t, J = 7.6 Hz, 2H), 2.34−2.24 (m, 6H), 1.82−1.80 (m, 2H). ESIMS: 502 $[M]^+$. HRFAB$^+$: calcd for $C_{72}H_{31}N_5O_{10}Re$, 772.1628; found, 772.1632.

Tricarbonyl(2-[3-(5-{7-[6-(Bis-pyridin-2-ylmethyl-amino)-hexylcarbamoyl]-heptanoylamino}-1-carboxy-pentyl)-ureido]-pentanedioic acid)rhenium bromide (ReL7). For HPLC purification, method 1 was used. R_t = 18.0 min. ^{1}H NMR (5/1 D_2O/CD_3CN): δ 9.43 (d, J = 5.2 Hz, 2H), 8.56 (t, J = 8.6 Hz, 2H), 8.10 (d, J = 7.6 Hz, 2H), 7.97 (t, J = 6.4 Hz, 2H), 5.38−5.29 (m, 4H), 4.80−4.35 (m, 2H), 3.80−3.72 (m, 5H), 3.05 (t, J = 7.6 Hz, 2H), 2.8−1.82 (m, 27H).

Radiochemistry. Compounds **L1**−**L7** were synthesized in radioactive (^{99m}Tc-labeled) form using the same general method as described below for [^{99m}Tc]**L1**. All Tc-99m-labeled compounds were synthesized in radiochemical yields of >70% and radiochemical purities of >98%. $[^{99m}Tc(CO)_3(H_2O)_3]^+$ preparation, typical example: 11.2 mCi (in 1 mL saline) $^{99m}TcO_4^-$ was added to the Isolink kit and the reaction mixture was heated in a water bath at 95 °C for 30 min then allowed to cool to room temperature. ^{99m}TcL preparation, typical example: 500 μL of the $[^{99m}Tc(CO)_3(H_2O)_3]^+$ solution (2.3 mCi) was neutralized with 50 μL 1(N) HCl. To this was added a 200 μL of phosphate-buffered saline (PBS) solution and 300 μL of a solution of **L1** (4 mg, 5.09 μmol in 2.5 mL water). This was kept at 95 °C for 30 min. The vial was cooled for 5 min at room temperature. This was diluted with 750 μL of the HPLC mobile phase and purified by radio-HPLC (method 1). The major radioactive peak constituting desired product (1.6 mCi) eluted at 14 min. The acidic eluate was neutralized with 100 μL 0.1 M $NaHCO_3$ solution and the volume was reduced to 400 μL, pH 8 under reduced pressure. This was diluted with PBS to the desired radioactivity concentration for ex vivo biodistribution and imaging studies. Radiochemical yield [^{99m}Tc]**L1**: 82.05%. Radiochemical purity = 98.99%.

Fluorescence Spectra. Fluorescence spectra were recorded using a Varian Cary Eclipse fluorescence spectrophotometer using with 321 nm excitation from a Xenon arc lamp. Compound Re**L2** was dissolved in ethylene glycol. Measurements were performed under air or after argon purging of the solution. Lifetime measurements were performed using a model D2, ISS, Inc. frequency domain spectrofluorimeter. The excitation wavelength was 370 nm from the UV LED. The fluorescence intensity data were collected through a bandpass filter in the spectral region 540−600 nm. Luminescence quantum yields were measured by the optical dilute method[57] using an aerated aqueous solution of $[Ru(bpy)_3]Cl_2$ (ϕ = 0.028, excitation wavelength at 455 nm)[58] as the standard solution.

NAALADase Assay. NAAG hydrolysis was performed essentially as described previously.[46,47] In short, LNCaP cell extracts were prepared by sonication in NAALADase buffer [50 mM Tris (pH 7.4) and 0.5% Triton X-100]. Cell lysates were incubated with or without inhibitor at 37 °C for 10 min. Following the incubation, the radiolabeled substrate *N*-acetyl-L-aspartyl-L-(3,4-^{3}H)glutamate (NEN Life Science Products, Boston, MA) was added to a final concentration of 30 nM at 37 °C for 10−15 min. The reaction was stopped by the addition of an equal volume of ice-cold 100 mM

sodium phosphate and 2 mM EDTA. Products were partitioned by AG 1-X8 formate resin (Bio-Rad Laboratories) anion exchange chromatography, eluted with 1 M sodium formate, and quantified by liquid scintillation counting. Inhibition curves were determined using semilog plots and IC_{50} values determined at the concentration at which enzyme activity was inhibited by 50%. Assays were performed in triplicate with the entire inhibition study being repeated at least once to confirm affinity and mode of inhibition. Data were collected during linear phase of hydrolysis (i.e., <20% cleavage of total substrate). Enzyme inhibitory constants (K_i values) were generated using the Cheng−Prusoff conversion.[59]

Cell Culture and Ex Vivo Biodistribution. PSMA+ PC3 PIP cells (human metastatic [bone] prostate carcinoma) engineered to express PSMA stably and PSMA− PC3 flu cells were generously provided by Warren Heston (Cleveland Clinic). Cells were cultured in T175 flasks using RPMI 1640 medium (Sigma) supplemented with 10% FBS and Penicillin/Streptomycin (100 U/mL/100 μg/mL) at 37 °C in 5% CO_2 in air. When a sufficient number of cells were present in culture, the cells were trypsinized and formulated in sterile Hanks buffered saline solution (Sigma, HBSS) and counted using a hemocytometer and trypan blue dye to confirm cell viability. Typically, $2-5 \times 10^6$ cells were injected subcutaneously such that PC3 PIP cells were injected behind the left shoulder and PC3 flu cells were injected behind the right shoulder of male severe-combined immunodeficient mice (SCID). All in vivo experimental procedures were undertaken in compliance with United States laws governing animal experimentation and were approved by the Johns Hopkins University Institutional Animal Care and Use Committee. Mice were used when the tumors reached 3−7 mm in diameter for either ex vivo biodistribution studies or in vivo SPECT-CT.

The xenograft-bearing mice (17−20 g) were injected via the tail vein with 3.70 MBq (100 μCi) of [^{99m}Tc]**L1**−**L4** in 200 μL of saline. Blood was collected immediately after sacrifice (cervical dislocation) by cardiac puncture and heart, lung, liver, stomach, pancreas, spleen, white fat, kidney, muscle, small intestine, large intestine, urinary bladder, and tumor xenografts were harvested, weighed, and counted in an automated gamma counter (LKB Wallace 1282 Compugamma CS Universal Gamma Counter). Animals were sacrificed at 30, 60, 120, and 300 min postinjection ($n = 4$ per time point). Tissue radiopharmaceutical uptake values were calculated as percent injected dose per gram (% ID/g) as compared with a 1:10 diluted standard dose. The urinary bladder was emptied and water washed and then dried prior to weighing and counting.

SPECT-CT Imaging of PC3 PIP and PC3 flu Xenografts. Compounds **L1**−**L4** were studied with imaging. Xenograft models were generated as described above. Mice were anesthetized using 1% isoflurane gas in oxygen flowing at 0.6 L/min prior to and during radiopharmaceutical injection. Mice were injected via the tail vein with approximately 480 μCi (17.76 MBq) of either **L1**, **L2**, **L3**, or **L4** formulated in 200 μL of PBS, pH 7. Allowing for 15 min of radiopharmaceutical uptake, anesthetized mice were placed on the scanner gantry and secured with medical tape while the anesthetic flow was increased to 0.8 L/min. Body temperature of the mice was maintained by covering them with several layers of Chux disposable pads in addition to keeping them illuminated with a dissection lamp during scanning. A Gamma Medica (Northridge, CA) X-SPECT scanner equipped with two opposing low-energy 0.5 mm aperature pinholes and tunable CT was used for all scans. Mice were scanned over 180° in 5.5°, 30 s increments. A CT scan was performed prior to scintigraphy for both anatomical coregistration and attenuation correction. Data were reconstructed and fused using commercial software from the vendor (Gamma Medica), which includes a 2D-OSEM algorithm.

In Vivo Binding Specificity (Blocking) Study. [^{99m}Tc]**L1** [1.1 mCi (40.7 MBq)] in 200 μL of saline was administered via the tail vein to an anesthetized animal bearing an LNCaP (PSMA+) tumor. Concurrently a second animal, also bearing an LNCaP tumor, was administered a cocktail containing 1.2 mCi (44.4 MBq) of [^{99m}Tc]**L1** and 1 mg of PMPA (Axxora Platform, San Diego, CA) in a total volume of 200 μL of saline. SPECT-CT imaging was then performed as described above, with both animals on the scanner gantry.

Metabolite Studies. Male CD-1 mice (Charles River Laboratories) were injected with 15 μCi (555 kBq) of [^{99m}Tc]**L1** in saline via the tail vein. Mice were sacrificed at either 30 min or 1 h postinjection by cervical dislocation and their blood and selected organs were removed. Blood samples were withdrawn using heparinized syringes, and tissues were placed on ice prior to manual homogenization in PBS, pH 7.4. Plasma and tissue homogenates in PBS were centrifuged for 2 min at 13000*g* at ambient temperature. A portion of the supernatant was diluted to 4 mL in 8 M urea containing 50 mg citric acid. Urine samples were added directly to 4 mL of the acidified urea solution. Samples then underwent separation by HPLC as previously described.[60] Briefly, the 4 mL sample in 8 M acidified urea was passed through a capture column (Strata-X, 19 mm × 4.4 mm, Phenomenex, Torrance, CA) at 2 mL/min followed by 1% acetonitrile in water to wash plasma proteins from the column. The effluent from the capture column, containing only highly polar components, flowed through a dual BGO detector (Bioscan, Washington, DC) operating in the diode mode. The solvent was then switched to 30% acetonitrile:50 mM phosphate buffer at pH 2.4 (2 mL/min) for elution of the radiolabeled components previously bound to the capture column onto the analytical column (Synergi Polar-RP 250 mm × 4.6 mm 10 μm particle size Phenomenex).

In Vitro Fluorescence Microscopy of ReL2 in PC3 PIP and PC3 flu Cells. Compound **L2**, when bound to the $[Re(I)(CO)_3]^+$ core, was hypothesized to be fluorescent as the corresponding bisquinoline chelator is known to have fluorescent properties.[30,39,40,61] Following fresh preparation of Re**L2**, 10000 PC3 PIP and PC3 flu cells were seeded separately into each of four wells of a Laboratory-Tek II 8-well chamber slide (Fisher Scientific). The cells were cultured as described above and were allowed to attach to the bottom of the wells overnight at 37 °C in 5% CO_2 in air. Serially diluted aliquots of Re**L2** were added to the media in six of the wells such that wells contained 500 nM, 250 nM or 125 nM Re**L2** with two remaining free of fluorophore. The cells were then returned to the incubator for one hour to enable binding. Each well was then carefully washed by removing the supernatant followed by addition of warm culture media for 30 s. The wash media was then removed and added to the contents of the well chambers. Dako Cytomation mounting medium was then applied and a glass coverslip was added. The mounting medium was allowed to dry at ambient temperature for 20 min prior to storage of the slide at 4 °C overnight. The cells were then viewed using an Olympus BX61 fluorescence microscope equipped with a Semrock DAPI/FITC/Texas Red triple filter cube. Excitation was at 494 nm with collection of emitted fluorescence at 628 nm.

Acknowledgment. This work was supported by NIH CA92871, CA1114111, EB005324, and the AdMeTech Foundation. We also thank Dr. Warren Heston for providing the PC3 PIP and flu cells.

Supporting Information Available: The procedure describing the molecular modeling studies, an overlay figure of **L1** with GPI-18413 (Supporting Information Figure 1) and a superimposed image of L1 before and after molecular dynamics simulation (Supporting Information Figure 2). This material is available free of charge via the Internet at http://pubs.acs.org.

References

(1) Jemal, A.; Murray, T.; Samuels, A.; Ghafoor, A.; Ward, E.; Thun, M. J. Cancer statistics, 2003. *Ca Cancer J. Clin.* **2003**, *53*, 5–26.
(2) Lange, P. H. PROSTASCINT scan for staging prostate cancer. *Urology* **2001**, *57*, 402–406.
(3) Haseman, M. K.; Rosenthal, S. A.; Polascik, T. J. Capromab pendetide imaging of prostate cancer. *Cancer Biother. Radiopharm.* **2000**, *15*, 131–140.
(4) Rosenthal, S. A.; Haseman, M. K.; Polascik, T. J. Utility of capromab pendetide (ProstaScint) imaging in the management of prostate cancer. *Tech. Urol.* **2001**, *7*, 27–37.

(5) Scher, B.; Seitz, M.; Albinger, W.; Tiling, R.; Scherr, M.; Becker, H. C.; Souvatzogluou, M.; Gildehaus, F. J.; Wester, H. J.; Dresel, S. Value of 11C-choline PET and PET/CT in patients with suspected prostate cancer. *Eur. J. Nucl. Med. Mol. Imaging* **2007**, *34*, 45–53.

(6) Rinnab, L.; Mottaghy, F. M.; Blumstein, N. M.; Reske, S. N.; Hautmann, R. E.; Hohl, K.; Moller, P.; Wiegel, T.; Kuefer, R.; Gschwend, J. E. Evaluation of [11C]-choline positron-emission/computed tomography in patients with increasing prostate-specific antigen levels after primary treatment for prostate cancer. *BJU Int.* **2007**, *100*, 786–793.

(7) Reske, S. N.; Blumstein, N. M.; Neumaier, B.; Gottfried, H. W.; Finsterbusch, F.; Kocot, D.; Moller, P.; Glatting, G.; Perner, S. Imaging prostate cancer with 11C-choline PET/CT. *J. Nucl. Med.* **2006**, *47*, 1249–1254.

(8) Zophel, K.; Kotzerke, J. Is 11C-choline the most appropriate tracer for prostate cancer? Against. *Eur. J. Nucl. Med. Mol. Imaging* **2004**, *31*, 756–759.

(9) Vees, H.; Buchegger, F.; Albrecht, S.; Khan, H.; Husarik, D.; Zaidi, H.; Soloviev, D.; Hany, T. F.; Miralbell, R. 18F-choline and/or 11C-acetate positron emission tomography: detection of residual or progressive subclinical disease at very low prostate-specific antigen values (<1 ng/mL) after radical prostatectomy. *BJU Int.* **2007**, *99*, 1415–1420.

(10) Larson, S. M.; Morris, M.; Gunther, I.; Beattie, B.; Humm, J. L.; Akhurst, T. A.; Finn, R. D.; Erdi, Y.; Pentlow, K.; Dyke, J.; Squire, O.; Bornmann, W.; McCarthy, T.; Welch, M.; Scher, H. Tumor localization of 16beta-18F-fluoro-5alpha-dihydrotestosterone versus 18F-FDG in patients with progressive, metastatic prostate cancer. *J. Nucl. Med.* **2004**, *45*, 366–373.

(11) Schuster, D. M.; Votaw, J. R.; Nieh, P. T.; Yu, W.; Nye, J. A.; Master, V.; Bowman, F. D.; Issa, M. M.; Goodman, M. M. Initial experience with the radiotracer anti-1-amino-3-18F-fluorocyclobutane-1-carboxylic acid with PET/CT in prostate carcinoma. *J. Nucl. Med.* **2007**, *48*, 56–63.

(12) Tehrani, O. S.; Muzik, O.; Heilbrun, L. K.; Douglas, K. A.; Lawhorn-Crews, J. M.; Sun, H.; Mangner, T. J.; Shields, A. F. Tumor imaging using 1-(2′-deoxy-2′−18F-fluoro-beta-D-arabinofuranosyl)thymine and PET. *J. Nucl. Med.* **2007**, *48*, 1436–1441.

(13) Mease, R. C.; Dusich, C. L.; Foss, C. A.; Ravert, H. T.; Dannals., R. F.; Seidel, J.; Prideaux, A.; Fox, J. J.; Sgouros, G.; Kozikowski, A. P.; Pomper, M. G. Synthesis and in vivo evaluation of *N*-[*N*-[(*S*)-1,3-dicarboxypropyl]carbamoyl]-4-[^{18}F]fluorobenzyl-L-cysteine, [^{18}F]DCFBC: a new imaging probe for prostate cancer. *Clin. Cancer Res.* **2008**, *14*, 3036–3043.

(14) Foss, C. A.; Mease, R. C.; Fan, H.; Wang, Y.; Ravert, H. T.; Dannals, R. F.; Olszewski, R.; Heston, W. D.; Kozikowski, A. P.; Pomper, M. G. Radiolabeled small molecule ligands for prostate-specific membrane antigen: in vivo imaging in experimental models of prostate cancer. *Clin. Cancer Res.* **2005**, *11*, 4022–4028.

(15) Pomper, M. G.; Musachio, J. L.; Zhang, J.; Scheffel, U.; Zhou, Y.; Hilton, J.; Maini, A.; Dannals, R. F.; Wong, D. F.; Kozikowski, A. P. 11C-MCG: synthesis, uptake selectivity, and primate PET of a probe for glutamate carboxypeptidase II (NAALADase). *Mol. Imaging* **2002**, *1*, 96–101.

(16) Zhou, J.; Neale, J. H.; Pomper, M. G.; Kozikowski, A. P. NAAG peptidase inhibitors and their potential for diagnosis and therapy. *Nat. Rev. Drug Discovery* **2005**, *4*, 1015–1026.

(17) Schulke, N.; Varlamova, O. A.; Donovan, G. P.; Ma, D.; Gardner, J. P.; Morrissey, D. M.; Arrigale, R. R.; Zhan, C.; Chodera, A. J.; Surowitz, K. G.; Maddon, P. J.; Heston, W. D.; Olson, W. C. The homodimer of prostate-specific membrane antigen is a functional target for cancer therapy. *Proc. Natl. Acad. Sci. U.S.A.* **2003**, *100*, 12590–12595.

(18) Chang, S. S.; Reuter, V. E.; Heston, W. D.; Bander, N. H.; Grauer, L. S.; Gaudin, P. B. Five different anti-prostate-specific membrane antigen (PSMA) antibodies confirm PSMA expression in tumor-associated neovasculature. *Cancer Res.* **1999**, *59*, 3192–3198.

(19) Nan, F.; Bzdega, T.; Pshenichkin, S.; Wroblewski, J. T.; Wroblewska, B.; Neale, J. H.; Kozikowski, A. P. Dual function glutamate-related ligands: discovery of a novel, potent inhibitor of glutamate carboxypeptidase II possessing mGluR3 agonist activity. *J. Med. Chem.* **2000**, *43*, 772–774.

(20) Tasch, J.; Gong, M.; Sadelain, M.; Heston, W. D. A unique folate hydrolase, prostate-specific membrane antigen (PSMA): a target for immunotherapy. *Crit. Rev. Immunol.* **2001**, *21*, 249–261.

(21) Alberto, R.; Schibli, R.; Egli, A.; Schubiger, A. P.; Abram, U.; Kaden, T. A. A novel organometallic aqua complex of technetium for the labeling of biomolecules: synthesis of [99mTc(OH2)3(CO)3]+ from [99mTcO4]−in aqueous solution and its reaction with a bifunctional ligand. *J. Am. Chem. Soc.* **1998**, *120*, 7987–7988.

(22) Alberto, R.; Ortner, K.; Wheatley, N.; Schibli, R.; Schubiger, A. P. Synthesis and properties of boranocarbonate: a convenient in situ CO source for the aqueous preparation of [(99m)Tc(OH(2))3(CO)3]+. *J. Am. Chem. Soc.* **2001**, *123*, 3135–3136.

(23) Banerjee, S. R.; Maresca, K. P.; Francesconi, L.; Valliant, J.; Babich, J. W.; Zubieta, J. New directions in the coordination chemistry of 99mTc: a reflection on technetium core structures and a strategy for new chelate design. *Nucl. Med. Biol.* **2005**, *32*, 1–20.

(24) Stephenson, K. A.; Banerjee, S. R.; Sogbein, O. O.; Levadala, M. K.; McFarlane, N.; Boreham, D. R.; Maresca, K. P.; Babich, J. W.; Zubieta, J.; Valliant, J. F. A new strategy for the preparation of peptide-targeted technetium and rhenium radiopharmaceuticals. The automated solid-phase synthesis, characterization, labeling, and screening of a peptide-ligand library targeted at the formyl peptide receptor. *Bioconjugate Chem.* **2005**, *16*, 1189–1195.

(25) Mesters, J. R.; Barinka, C.; Li, W.; Tsukamoto, T.; Majer, P.; Slusher, B. S.; Konvalinka, J.; Hilgenfeld, R. Structure of glutamate carboxypeptidase II, a drug target in neuronal damage and prostate cancer. *EMBO J.* **2006**, *25*, 1375–1384.

(26) Mesters, J. R.; Henning, K.; Hilgenfeld, R. Human glutamate carboxypeptidase II inhibition: structures of GCPII in complex with two potent inhibitors, quisqualate and 2-PMPA. *Acta Crystallogr., Sect. D: Biol. Crystallogr.* **2007**, *63*, 508–513.

(27) Barinka, C.; Rovenska, M.; Mlcochova, P.; Hlouchova, K.; Plechanovova, A.; Majer, P.; Tsukamoto, T.; Slusher, B. S.; Konvalinka, J.; Lubkowski, J. Structural insight into the pharmacophore pocket of human glutamate carboxypeptidase II. *J. Med. Chem.* **2007**, *50*, 3267–3273.

(28) Barinka, C.; Starkova, J.; Konvalinka, J.; Lubkowski, J. A high-resolution structure of ligand-free human glutamate carboxypeptidase II. *Acta Crystallogr., Sect. F: Struct. Biol. Cryst. Commun.* **2007**, *63*, 150–153.

(29) Tooyama, Y.; Harano, A.; Yoshimura, T.; Takayama, T.; Sekine, T.; Kudo, H.; Shinohara, A. Synthesis, structure, and spectroscopic properties of fac-[TcICl(CO)3(bpy)] (bpy = 2,2′-bipyridine). *J. Nucl. Radiochem. Sci.* **2005**, *6*, 153–155.

(30) Banerjee, S. R.; Babich, J. W.; Zubieta, J. Site directed maleimide bifunctional chelators for the M(CO)3+ core (M = (99m)Tc, Re). *Chem. Commun. (Cambridge)* **2005**, 1784–1786.

(31) Maclaren, J. A. A convenient preparative method for esters of amino acids. *Austr. J. Chem.* **1972**, *25*, 1293–1299.

(32) Maclaren, J. A. Some amino acid esters: An improved preparative method. *Austr. J. Chem.* **1978**, *31*, 1865–1868.

(33) Goodacre, J.; Ponsford, R. J.; Stirling, I. Selective removal of the *t*-butyloxycarbonyl protecting group in the presence of *t*-butyl and *p*-methoxybenzyl esters. *Tetrahedron Lett.* **1975**, *42*, 3609–3612.

(34) Goodacre, J.; Jeffries, L.; Nayler, J. H.; Ponsford, R. J.; Stirling, I. Antibacterial halogenoacetyl derivatives of amino acids and simple peptides. *J. Med. Chem.* **1977**, *20*, 1445–1448.

(35) Levadala, M. K.; Banerjee, S. R.; Maresca, K. P.; Babich, J. W.; Zubieta, J. Synthesis of bifunctional chelates for nuclear imaging. *Synthesis* **2004**, *11*, 1759–1766.

(36) Mueller, C.; Dumas, C.; Hoffmann, U.; Schubiger, A. P.; Schibli, R. Organometallic 99mTc-technetium(I)- and Re-rhenium(I)-folate derivatives for potential use in nuclear medicine. *J. Organomet. Chem.* **2004**, *689*, 4712–4721.

(37) Lazarova, N.; James, S.; Babich, J. W.; Zubieta, J. A convenient synthesis, chemical characterization and reactivity of [Re(CO)3(H2O)3]Br: the crystal and molecular structure of [Re(CO)3(CH3CN)2Br]. *Inorg. Chem. Commun.* **2004**, *7*, 1023–1026.

(38) Mlcochova, P.; Plechanovova, A.; Barinka, C.; Mahadevan, D.; Saldanha, J. W.; Rulisek, L.; Konvalinka, J. Mapping of the active site of glutamate carboxypeptidase II by site-directed mutagenesis. *FEBS J.* **2007**, *274*, 4731–4741.

(39) Stephenson, K. A.; Banerjee, S. R.; Besanger, T.; Sogbein, O. O.; Levadala, M. K.; McFarlane, N.; Lemon, J. A.; Boreham, D. R.; Maresca, K. P.; Brennan, J. D.; Babich, J. W.; Zubieta, J.; Valliant, J. F. Bridging the gap between in vitro and in vivo imaging: isostructural Re and 99mTc complexes for correlating fluorescence and radioimaging studies. *J. Am. Chem. Soc.* **2004**, *126*, 8598–8599.

(40) James, S.; Maresca, K. P.; Babich, J. W.; Valliant, J. F.; Doering, L.; Zubieta, J. Isostructural Re and 99mTc complexes of biotin derivatives for fluorescence and radioimaging studies. *Bioconjugate Chem.* **2006**, *17*, 590–596.

(41) Di Bilio, A. J.; Crane, B. R.; Wehbi, W. A.; Kiser, C. N.; Abu-Omar, M. M.; Carlos, R. M.; Richards, J. H.; Winkler, J. R.; Gray, H. B. Properties of photogenerated tryptophan and tyrosyl radicals in structurally characterized proteins containing rhenium(I) tricarbonyl diimines. *J. Am. Chem. Soc.* **2001**, *123*, 3181–3182.

(42) Guo, X. Q.; Castellano, F. N.; Li, L.; Lakowicz, J. R. Use of a long-lifetime Re(I) complex in fluorescence polarization immunoassays of high-molecular-weight analytes. *Anal. Chem.* **1998**, *70*, 632–637.

(43) Guo, X. Q.; Castellano, F. N.; Li, L.; Szmacinski, H.; Lakowicz, J. R.; Sipior, J. A long-lived, highly luminescent Re(I) metal-ligand complex as a biomolecular probe. *Anal. Biochem.* **1997**, *254*, 179–186.
(44) Lo, K. K.; Tsang, K. H.; Hui, W. K.; Zhu, N. Luminescent rhenium(I) diimine indole conjugates: photophysical, electrochemical and protein-binding properties. *Chem. Commun. (Cambridge)* **2003**, 2704–2705.
(45) Dattelbaum, J. D.; Abugo, O. O.; Lakowicz, J. R. Synthesis and characterization of a sulfhydryl-reactive rhenium metal−ligand complex. *Bioconjugate Chem.* **2000**, *11*, 533–536.
(46) Robinson, M. B.; Blakely, R. D.; Couto, R.; Coyle, J. T. Hydrolysis of the brain dipeptide *N*-acetyl-L-aspartyl-L-glutamate. Identification and characterization of a novel N-acetylated alpha-linked acidic dipeptidase activity from rat brain. *J. Biol. Chem.* **1987**, *262*, 14498–14506.
(47) Lupold, S. E.; Hicke, B. J.; Lin, Y.; Coffey, D. S. Identification and characterization of nuclease-stabilized RNA molecules that bind human prostate cancer cells via the prostate-specific membrane antigen. *Cancer Res.* **2002**, *62*, 4029–4033.
(48) Slusher, B. S.; Tsai, G.; Yoo, G.; Coyle, J. T. Immunocytochemical localization of the *N*-acetyl-aspartyl-glutamate (NAAG) hydrolyzing enzyme N-acetylated alpha-linked acidic dipeptidase (NAALADase). *J. Comp. Neurol.* **1992**, *315*, 217–229.
(49) Rajasekaran, S. A.; Anilkumar, G.; Oshima, E.; Bowie, J. U.; Liu, H.; Heston, W.; Bander, N. H.; Rajasekaran, A. K. A novel cytoplasmic tail MXXXL motif mediates the internalization of prostate-specific membrane antigen. *Mol. Biol. Cell* **2003**, *14*, 4835–4845.
(50) Moffatt, S.; Papasakelariou, C.; Wiehle, S.; Cristiano, R. Successful in vivo tumor targeting of prostate-specific membrane antigen with a highly efficient J591/PEI/DNA molecular conjugate. *Gene Ther.* **2006**, *13*, 761–772.
(51) Jackson, P. F.; Cole, D. C.; Slusher, B. S.; Stetz, S. L.; Ross, L. E.; Donzanti, B. A.; Trainor, D. A. Design, synthesis, and biological activity of a potent inhibitor of the neuropeptidase N-acetylated alpha-linked acidic dipeptidase. *J. Med. Chem.* **1996**, *39*, 619–622.
(52) Sodee, D. B.; Sodee, A. E.; Bakale, G. Synergistic value of single-photon emission computed tomography/computed tomography fusion to radioimmunoscintigraphic imaging of prostate cancer. *Semin. Nucl. Med.* **2007**, *37*, 17–28.
(53) Milowsky, M. I.; Nanus, D. M.; Kostakoglu, L.; Sheehan, C. E.; Vallabhajosula, S.; Goldsmith, S. J.; Ross, J. S.; Bander, N. H. Vascular targeted therapy with anti-prostate-specific membrane antigen monoclonal antibody J591 in advanced solid tumors. *J. Clin. Oncol.* **2007**, *25*, 540–547.
(54) Nargund, V.; Al Hashmi, D.; Kumar, P.; Gordon, S.; Otitie, U.; Ellison, D.; Carroll, M.; Baithun, S.; Britton, K. E. Imaging with radiolabelled monoclonal antibody (MUJ591) to prostate-specific membrane antigen in staging of clinically localized prostatic carcinoma: comparison with clinical, surgical and histological staging. *BJU Int.* **2005**, *95*, 1232–1236.
(55) Kozikowski, A. P.; Nan, F.; Conti, P.; Zhang, J.; Ramadan, E.; Bzdega, T.; Wroblewska, B.; Neale, J. H.; Pshenichkin, S.; Wroblewski, J. T. Design of remarkably simple, yet potent urea-based inhibitors of glutamate carboxypeptidase II (NAALADase). *J. Med. Chem.* **2001**, *44*, 298–301.
(56) Banerjee, S. R.; Wei, L.; Levadala, M. K.; Lazarova, N.; Golub, V. O.; O'Connor, C. J.; Stephenson, K. A.; Valliant, J. F.; Babich, J. W.; Zubieta, J. [Re(III)Cl(3)] core complexes with bifunctional single amino acid chelates. *Inorg. Chem.* **2002**, *41*, 5795–5802.
(57) Nakamura, K. Synthesis, luminescence quantum yields, and lifetimes of trischelated ruthenium(II) mixed-ligand complexes including 3,3′-dimethyl-2,2′-bipyridyl. *Bull. Chem. Soc. Jpn.* **1982**, *55*, 2697–2705.
(58) Crosby, G. A.; Demas, J. N. Measurement of photoluminescence quantum yields. *J. Phys. Chem.* **1971**, *75*, 991–1024.
(59) Cheng, Y.; Prusoff, W. H. Relationship between the inhibition constate (K1) and the concentration of inhibitor which causes 50% inhibition (I50) of an enzymatic reaction. *Biochem. Pharmacol.* **1973**, *22*, 3099–3108.
(60) Hilton, J.; Yokoi, F.; Dannals, R. F.; Ravert, H. T.; Szabo, Z.; Wong, D. F. Column-switching HPLC for the analysis of plasma in PET imaging studies. *Nucl. Med. Biol.* **2000**, *27*, 627–630.
(61) Banerjee, S. R.; Babich, J. W.; Zubieta, J. A new bifunctional amino acid chelator targeting the glucose transporter. *Inorg. Chim. Acta* **2006**, *359*, 1603–1612.

JM800111U